LBNL-41192

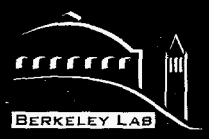

ERNEST ORLANDO LAWRENCE
BERKELEY NATIONAL LABORATORY

Environmental Management Science Program Awards

Fiscal Year 1997 Annual Progress Report

Ardyth Simmons, Editor

Earth Sciences Division

October 1997

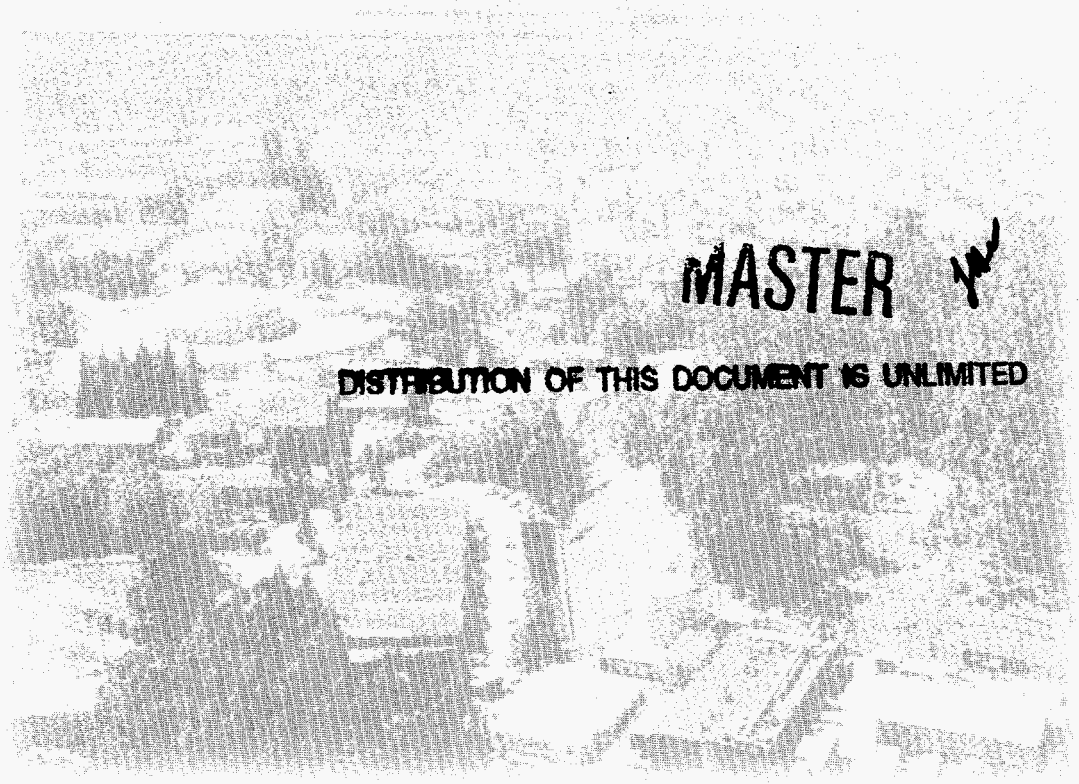

LBNL-41182

Lawrence Berkeley National Laboratory Environmental Management Science Program Awards

EMSP

Fiscal Year 1997 Annual Progress Report

W. Henry Benner, Donald J. DePaolo,
Boris Faybishenko, E.L. Majer, Maria Pallavicini,
Richard E. Russo, Peter G. Shultz and Jiamin Wan

Edited by
Ardyth Simmons

October 1997

Acknowledgement
This work was supported by the Environmental Management Science Program managed by the partnership of the Office of Environmental Management, and the Office of Energy Research, U.S. Department of Energy, under Contract No. DE-AC03-76SF00098.

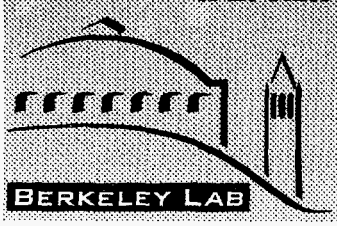

ERNEST ORLANDO LAWRENCE
BERKELEY NATIONAL LABORATORY

Lawrence Berkeley National Laboratory
EMSP Annual Progress Report - October 1997

Table of Contents

Lawrence Berkeley National Laboratory
Environmental Management Science Program

Executive Summary

October 31, 1997

Lawrence Berkeley National Laboratory was awarded eight Environmental Management Science Program (EMSP) research grants in Fiscal Year 1996. This report summarizes the progress of each grant in addressing significant DOE site cleanup issues after completion of the first year of research. The technical progress made to date in each of the research projects is described in greater detail in the following individual progress reports. The focus of the research projects covers a diversity of areas relevant to site cleanup, including bioremediation, health effects, characterization, and mixed waste. Some of the projects cut across a number of focus areas. Three of the projects are directed toward characterization and monitoring at the Idaho National Engineering and Environmental Laboratory, as a test case for application to other sites.

MIXED WASTE/REMEDIATION

Gas-water interfaces often play a role in transport processes. The EMSP project, **Sorption of Colloids, Organics, and Metals onto Gas-Water Interfaces: Transport Processes and Potential Remediation Technology** is aimed at improving the basic understanding of contaminant interactions with gas-water interfaces, with emphasis on the behavior of mixed contaminant systems. Its second objective is to develop a sorptive microbubble fractionation remediation technique. Quantification and visualization at both micro- and macro-scales is underway to test three hypotheses that support these objectives. In principle, sorptive bubble and microbubble separation techniques can be employed for removing any contaminants that partition favorably at gas-liquid interfaces, when environments do not severely constrain bubble or microbubble movement.

In this first year of research, an improved understanding of contaminant sorption at gas-water interfaces was obtained by developing a sorptive bubble column method for quantifying surface excesses of contaminants under dynamic conditions. Furthermore, humic acid sorption at air-water interfaces was quantified under dynamic conditions, and the first quantitative measurements of clay colloid sorption at these interfaces were obtained. Surfactant combinations were identified that provide microbubbles with different surface characteristics. Also the stability of microbubble suspensions was optimized and initial tests of microbubble transport in sand columns were completed. One main area of focus in upcoming experiments is that of identifying surfactants that are highly selective for specific contaminants. In subsurface environments, the *in situ* microbubble technique is expected to permit access to contaminated zones that are not pore size-restrictive.

BIOREMEDIATION

Rapid Mass Spectrometric DNA Diagnostics for Assessing Microbial Community Activity During Bioremediation is directed toward developing rapid analytical instrumentation for DNA-based identification of bioremedial genes in soils and groundwater. The diagnostic procedures under evaluation are designed to identify specific genes in soil microorganisms that code for pollutant-degrading enzymes. Current DNA-based diagnostic procedures rely on gel electrophoresis as a way to identify members of the microbial population. This study is attempting to implement time-of-flight (TOF) mass spectrometry as a replacement for gel separations because of TOF's speed and potential for sample automation. If TOF techniques can be implemented effectively, a large number of microorganisms and soil samples can be screened for the presence of specific pollutant-degrading genes.

This year a demonstration test was completed that can be used to detect a specific gene in a pollutant-degrading organism. A set of primers and primer-binding conditions were determined using gene sequencing to replicate a particular region using a polymerase chain reaction (PCR). Secondly, the possible application of charge detection mass spectrometry (CDMS) was tested as a tool for detecting large PCR products. When applied to PCR products in the megadalton size range, a mass measurement provides a way to determine the size of the DNA strand. Mass measurements can be acquired from as few as 1000 ions in 10 minutes. When this procedure is compared to the several hours needed to separate the PCR product on an electrophoresis gel, the time saving is very significant. The assay being developed is specific to naphthalene and can be used to track the bioremediation of naphthalene. This study will be directed toward transforming the technique into a more general procedure that can be applied to the investigation of other pollutants and their degradation pathways.

The focus of **Enzyme Engineering for Biodegradation of Chlorinated Organic Pollutants** is on the development of tailor-made biological catalysts for modifying or degrading halogenated compounds and other environmental pollutants. Catalytic antibodies not only selectively bind but also chemically transform virtually any molecule of interest. These enzymes could be used by themselves or could be inserted into microorganisms designed for high activity in contaminated environments. The initial goal is to develop powerful new methods for screening or selecting catalytic antibodies from large antibody libraries. At present, libraries of variable region mutants are being generated by DNA shuffling. In addition, an amide derivative of the substrate is being synthesized, which when hydrolyzed will release indigo, providing a chromogenic assay of catalytic activity that can be used in a plate screen of libraries of mutants. If successful, the experiments will provide a general strategy for evolving protein catalysts with a broad range of specificities and activities. These approaches will then be directly

applied to the generation of antibodies that catalyze the hydrolysis of halogenated aromatics.

CHARACTERIZATION

Evaluation of Isotopic Diagnostics for Subsurface Characterization and Monitoring is directed toward field sites at the Test Area North (TAN) and the subsurface disposal area of the Radioactive Waste Management Complex (RWMC) at the Idaho National Engineering and Environmental Laboratory (INEEL). Isotopic measurements such as ^{13}C, ^{14}C, ^{3}He, ^{87}Sr, ^{37}Cl, and ^{18}O, which are present in groundwater and soil gas, can be used to identify the sites of origin of contaminants in groundwater and to determine if contaminants are being degraded as a result of natural or engineered processes. Isotope ratios also can be used to trace the migration of fluids that are pumped down wells to degrade or contain underground contaminants, such as steam and grout, as well as to diagnose what chemical reactions are occurring underground.

At the TAN site, a combination of low-level radioactive isotopes, sewage, and chlorinated solvents was disposed of in a 310-ft well that penetrates the Snake River Aquifer. Presently a pump-and-treat system is removing small quantities of TCE. Reduction of the plume to below the MCL for TCE may require some additional form of *in situ* degradation of TCE unless natural attenuation is demonstrated to be sufficient. Isotopic measurements are helping to decipher which reactions are occurring and whether contaminants are being degraded.

At the RWMC, volatile organic compound (VOC) contaminants are present in the vadose zone; their source is organic waste that was disposed of in pits and trenches. Present remedial activities use vapor extraction to withdraw contaminants; therefore successful remediation depends on understanding vapor flow in the vadose zone. Isotopic measurements are being used to understand subsurface flow, and to detect whether VOCs are being continually released as they are being pumped out, at what rate they are being pumped, and whether the VOCs are being naturally remediated by biological activity or other reactions. Preliminary results of isotopic analyses indicate that there is a substantial production of CO_2 in the subsurface of the RWMC site. Vadose zone CO_2 has a low $^{13}C/^{12}C$ ratio and therefore appears to be an oxidation product of organic material. However, initial ^{14}C analyses of the CO_2 indicate the presence of an additional, radioactive source for the CO_2.

Understanding subsurface flow and transport processes is critical for effective assessment, decision-making, and remediation activities for contaminated sites. However, for fluid flow and contaminant transport through fractured vadose zones, traditional hydrogeological approaches are often found to be inadequate. In **A Chaotic-Dynamical Conceptual Model to Describe Fluid Flow and Contaminant Transport in a Fractured Vadose Zone,** flow and transport are examined as a deterministic chaotic

dynamical process. The geometry and flow dynamics will eventually be merged to develop a chaotic-dynamical model of flow and transport in a fractured vadose zone. Water flow and contaminant transport are being investigated on several scales, ranging from small-scale laboratory experiments in fracture replicas and fractured cores, to field experiments conducted in a single exposed fracture at a basalt outcrop, and finally to a ponded infiltration test at the Box Canyon, Idaho analog site. The measured time-variation of water flux, moisture content, and hydraulic head at various locations, as well as the total inflow rate to the subsurface, reflect changes in the geometry and physics of water flow that may display chaotic behavior. In the analysis of experimental data, a chaotic model can be used to predict the long-term bounds on fluid flow and transport behavior and to examine the limits of short-term predictability within these bounds. This approach is well suited to the need for short-term predictions to support remediation decisions and long-term bounding studies.

High-Resolution Definition of Subsurface Heterogeneity for Understanding the Biodynamics of Natural Field Systems: Advancing the Ability for Scaling to Field Conditions uses innovative geophysical imaging and microbial characterization methods to identify key scales of physical heterogeneities that affect the biodynamics of natural subsurface environments. Data from controlled laboratory and *in situ* experiments at the INEEL TAN site are being used to determine the dominant lithologic, structural, and hydrologic characteristics that can be imaged *in situ* and correlated with microbial properties. This work is one of the building blocks of an integrated and collaborative approach with an INEEL/PNNL (Pacific Northwest National Laboratory) effort aimed at understanding the interrelationships between transport properties and spatially varying physical, chemical, and microbiological heterogeneity. The work addresses issues that will aid in understanding what scales must be sampled in order to design effective remediation strategies. A specific goal is to understand how to use geophysical imaging to predict the effect of physical heterogeneity and fluid transport properties on microbial behavior.

To date, cross-well geophysical measurements have been made to assess the continuity and homogeneity of the intervening material at the TAN site. During 1997 cross-well seismic data obtained at the sub-meter resolution scale indicated that the geology of the surveyed area is varied, with large changes in seismic velocity and attenuation with depth. In all well pairs the tomography has given good resolution on structure and possible areas of fast fluid-flow paths. Further analysis and correlation with other data should yield more definitive results on the identification of permeable pathways and structure controlling transport. With respect to microbial characterization and scale effects, DNA was extracted and successfully amplified from nine rock samples from the TAN-37 borehole. Time-course degradation of organic substrates in the presence and absence of additional organic and inorganic nutrients was performed on a number of samples and analysis is underway.

Chemical characterization is a top priority need in every DOE EM major problem area. Millions of dollars have been invested to utilize laser ablation technology to address chemical characterization needs within these problem areas. The project **Improved Analytical Characterization of Solid Waste Forms by Fundamental Development of the Laser Ablation Technology** addresses fundamental issues that must be understood to provide confidence in deployment of the technology. These include energy coupling, mass removal, gas dynamics, and transport. Energy coupling is critical in that it governs the sensitivity and accuracy of constituent removal. Experiments will provide new knowledge on space charge effects, plasma screening, and plasma expansion. Solid vapor entrainment and particle size distribution generated during laser ablation influences transport.

During this initial year of research, three important components of laser ablation sampling were demonstrated. The first component of the study demonstrated that the ICP-AES (inductively coupled plasma-atomic emission spectroscopy) technology is accurately responding to the chemical composition. As the laser beam properties and thereby the ablation conditions changed, the plasma conditions remained constant, proving for the first time that the ICP can be used for accurate chemical analysis over a wide range of laser operating conditions. The second study demonstrated that the quantity and composition of ablated mass changes over time as the laser repetitively removes mass from the sample. The quantity of ablated mass and its composition strongly depend on the number of laser pulses and laser fluence at the sample surface. This is important because the reported chemical composition can be greatly influenced by time and laser power density. The third study demonstrated how the efficiency of laser sampling can be improved by using a different gas in the ablation chamber. Of the noble gases tried, helium provided the greatest enhancement, due to a combination of the effect of higher He mixed gas, ICP temperature, and laser sampling efficiency.

HEALTH EFFECTS

Another study is **Environmentally-Induced Malignancies: An *In Vivo* Model to Evaluate the Health Impact of Chemicals in Mixed Waste.** Long-term health effects of exposure to complex mixtures of chemicals are of particular concern because their biologic effects may synergize to increase risk of malignancy in developing leukemia. Multiple chromosome abnormalities are present in the majority of leukemias. Accumulation of multiple genetic aberrations may reflect genomic instability in the affected cells. Agents that induce DNA damage or genomic instability may increase accumulation of genomic alterations, thereby predisposing cells to transformation. A progression model of environmentally induced leukemia is being evaluated that uses mouse models. The model postulates that mixtures of chemicals that kill blood cells and are genotoxic will synergize to increase the frequency of cells with genomic changes, and thus increase the risk of transformation. Normally quiescent stem cells are introduced into the cycle following hemotoxic insult, thereby facilitating generation of progeny with

altered genomes. Chemicals that increase the rate of genomic instability in stem cells are likely to increase the frequency of future stem cells with altered genomes. Mice have been treated with a cancer therapeutic to recruit cells into the cycle. In addition, benzene and its metabolites are being investigated to determine whether they induce translocations in stem cells in a dose-dependent manner. Data generated in this project will not only lend insight into mechanisms underlying environmental-induction of leukemic progression, but will facilitate development of a rationale to identify chemical combinations that increase or decrease leukemogenic potential and will provide opportunities to optimize approaches for biomonitoring and risk assessment.

Acknowledgement

This work was supported by the Environmental Management Science Program managed by the partnership of the Office of Environmental Management Science and the Office of Energy Research, U.S. Department of Energy under Contract No. DE-AC03-76SF00098.

For more information contact:

Dr. Sally M. Benson
Director, Earth Sciences Division
Lawrence Berkeley National Laboratory
(510) 486-5875

Dr. Ardyth M. Simmons
Technical Coordinator, Environmental
Remediation Technology
Lawrence Berkeley National Laboratory
(510) 486-7106

Sorption of Colloids, Organics, and Metals onto Gas-Water Interfaces: Transport Processes and Potential Remediation Technology

Principal Investigator:
Jiamin Wan, Tel: 510/495-6004, Fax: 510/486-5686, email: jwan@lbl.gov

Lawrence Berkeley National Laboratory
Mail Stop 90-1116

Co-Investigators: Tetsu K. Tokunaga (LBNL)
Fred Gadelle (LBNL)

1.0 Project Objectives

This research project has two objectives. The first is to improve basic understanding of contaminant interactions with gas - water interfaces, with emphasis on behavior of mixed contaminant systems. The second objective is to develop a sorptive microbubble fractionation remediation technique. Hypotheses supporting these objectives are: 1) contaminants and natural organics can sorb on and alter the interface hydrophobicity of the gas-water interfaces, and therefore influence sorption of colloids, metals, and radionuclides at gas-water interfaces; 2) surfactants can vastly increase sorption of colloids, metals and radionuclides selectively onto gas-water interfaces; 3) a sorptive microbubble fractionation remediation technique can be developed based on understanding of the previously mentioned processes. These hypotheses are being tested through quantification and visualization at both micro- and macro-scales.

2.0 Outline of Progress to Date

2.1 Improve Understanding of Contaminant Sorption at Gas-Water Interfaces (Objective #1)

- Developed a sorptive bubble column method for quantifying surface excesses of contaminants under dynamic conditions
- Related surface excesses measured with this new method to those measured using classic surface tension measurements
- Quantified humic acid sorption at air-water interfaces under dynamic conditions
- Obtained the first quantitative measurements of clay colloid sorption at air-water interfaces
- In progress: Quantification of metal-humic and metal-clay complexes on air-water interfaces

2.2 Develop a New Remediation Technique Based on Contaminant Sorption at Gas-Water Interfaces (Objective #2)

- Developed techniques for generating stable microbubbles (micrometer-scale):
  - spinning disk
  - ultrasonic probe

- Identified several surfactant combinations that provide microbubbles with different surface charge characteristics:

- Span60/Tween80
- Span60/SDS
- Span60/CTAB

- Optimized stability of microbubble suspensions having typical microbubble suspension characteristics as follows:
  - size: 1 - 2 μm
  - concentration: 10^7 - 10^8 per mL
  - interfacial area: ~ 3 - 13 cm^2 per mL
  - lifetime: in progress, one system now stable for at least 14 days

- Completed initial tests of microbubble transport in sand columns:
  - Slight microbubble retardation occurs during advective transport
  - Strong microbubble retardation/filtration occurs in hydrostatic columns

- Upcoming research activities:
  - Identification of microbubble surfactants that efficiently sorb metals and other contaminants
  - Microbubble sorptive extraction of contaminants in laboratory columns

3.0 Potential Applications

In principle, sorptive bubble and microbubble separation techniques can be employed for removing any contaminants that partition favorably at gas-liquid interfaces, in environments that do not severely constrain bubble or microbubble movement. One main area of focus in our upcoming experiments is that of identifying surfactants that are highly selective for specific contaminants. In subsurface environments, the *in situ* microbubble technique is expected to permit access to contaminated zones that are not pore size-restrictive. Thus, aquifer strata comprised of sands or gravel will be accessible. The lower grain-size limit is expected to be encountered in the fine sand to silt class. We also noted in our proposal that the sorptive, mobile gas-liquid interface might be useful in separations in waste tanks. In such an application, either microbubbles or bubbles could be used, since pore-size limitations do not exist. Factors that will determine applicability of this remediation approach include the level of contaminant-surfactant selectivity, microbubble (or bubble) stability and mobility, cost of surfactants, and development of microbubble (or bubble) collection-treatment methods.

4.0 Detailed Progress and Results

4.1 Sorptive Bubble Column Method for Quantifying Surface Excesses

Since groundwater systems are dynamic, heterogeneous, open environments, their gas-water interfaces can be in disequilibrium with respect to sorption of hydrophobic and surface active compounds. Thus, the traditional method of quantifying surface excesses by measuring changes in surface tension may only provide equilibrium-limit information. Furthermore, surface tension measurements are not sensitive to certain components that can be complexed with hydrophobic, surface-active species at the air-water interface. The nonfoaming bubble fractionation method provides an alternative approach to determining surface excesses. It was originally developed for industrial applications by Lemlich (1966) and Shah and Lemlich (1970) for separating surface-

active agents from dilute solutions. The method is based on the preferential adsorption of the surface-active compounds onto the interface of rising gas bubbles. Gas is bubbled through a vertical column containing the dilute aqueous solution of the surface-active agent. The rising bubbles adsorb and carry the surface-active agent to the top of the column, and release the sorbed component back to the solution when the bubbles burst. A concentration profile is established along the column length that, at steady-state, reflects the balance between upwards transport by sorption onto rising bubbles and downward transport by eddy dispersion. In this study, we further develop the bubble fraction column method in several ways. We first experimentally determined bubble column eddy dispersion coefficients, rather than assuming certain functional relations to column parameters. We then quantitatively compared surfactant partitioning in bubble columns with surface tension measurements. Finally, our main contribution is in applying the bubble fraction column method to the problem of quantifying partitioning of components at water - air interfaces, such as colloids and metals, which cannot be quantified by the surface tension method.

Before the bubble column method can be used reliably in quantifying surface excesses, an independent determination of the column dispersion coefficient is needed. It should be pointed out that no previous accounts of this method have included actual measurements of column dispersivities. Instead, previous researchers assumed certain functional relations and calculated dispersivities. The "measured" surface excesses in the bubble column method are very sensitive to errors introduced through assumed dispersivities. In our work, the eddy dispersivity was independently determined through electrical conductivity measurements of transient dispersion of NaCl pulses in bubble columns. Measured conductance time series were fit to the appropriate analytical solution of the diffusion equation, with the dispersivity as the fitting parameter. Our results show that previous researchers assumed dispersivities that were far too small.

It is important to understand whether or not steady-state concentration profiles in bubble columns reflect true equilibrium with respect to surface excesses on bubbles. For this purpose, we compared adsorption isotherms of surfactants Triton X-100, and sodium dodecyl benzene sulfonate at very dilute concentrations using both surface tension and bubble column methods. We found that surfactant partitioning at bubble interfaces in the dynamic column method amounted to only about 20% relative to equilibrium conditions (surface tension measurements). An article describing the bubble fraction column technique and applications is in preparation.

Our first environmental application of the bubble fractionation column involved measurements of humic acid partitioning at gas-water interfaces. Although several previous studies have investigated accumulation of humic substances at air-water interfaces via surface tension measurements, most of these previous experiments were conducted at concentrations that are much higher than those typically found in soil pore waters and groundwaters. Our recent bubble fraction column results quantify humic substance partitioning at moving air-water interfaces over a range of concentrations typical to subsurface environments. Figure 1 is an example of a typical relative concentration profile along a column. In this example, the solution initial concentration is 10 mg/L of humic acid (IHSS Soil Standard Humic Acid), pH 5.7, and ionic strength 5.0 mM. The points are measured steady-state concentrations along the column from five repeated runs, and the curve is the model-predicted concentration profile. The model does not account for the very high humic acid concentration within the thin film at the top of the column. The large variation of data from the surface layer in repeated runs is probably due to different extents of mixing with the underlying bulk solution during sampling. The only fitting parameter is K, the steady-state adsorption isotherm constant. The K value is 8.5E-6 m in this case.

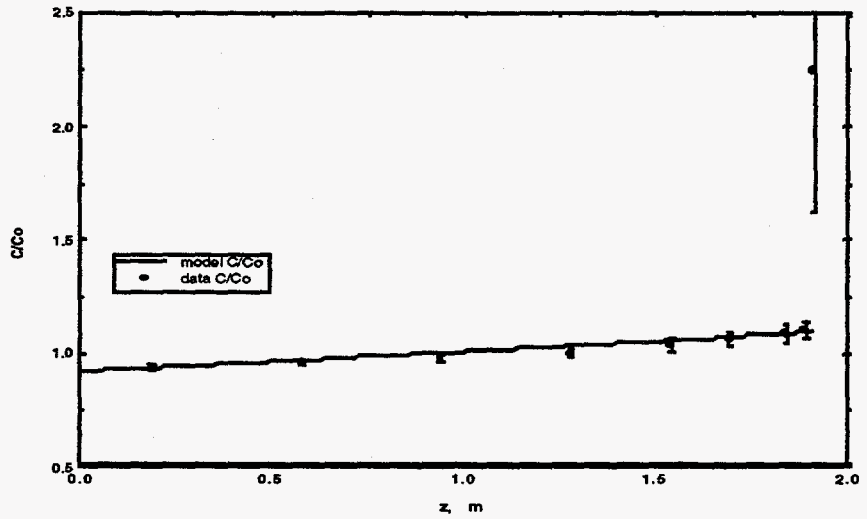

Figure 1. Steady-state relative concentration profile of humic acid in the bubble fraction column where C/Co = ratio of concentration in column (c) to initial concentration (Co).

The bubble fraction column method has very recently been used to obtain the first quantitative measurements of clay mineral sorption at gas-water interfaces. This previously unrecognized phenomenon was first observed by Wan and Wilson (1994), and has considerable relevance in colloid-facilitated contaminant transport. The steady-state concentration profile of kaolinite clay in the bubble fraction column clearly reveals favorable partitioning at gas-water interfaces (Figure 2). It is important to note that such partitioning is probably impossible to determine through surface tension measurements. Upcoming experiments will determine the extent to which metals and organic contaminants partition at gas-water interfaces through complexation with humic substances and clays.

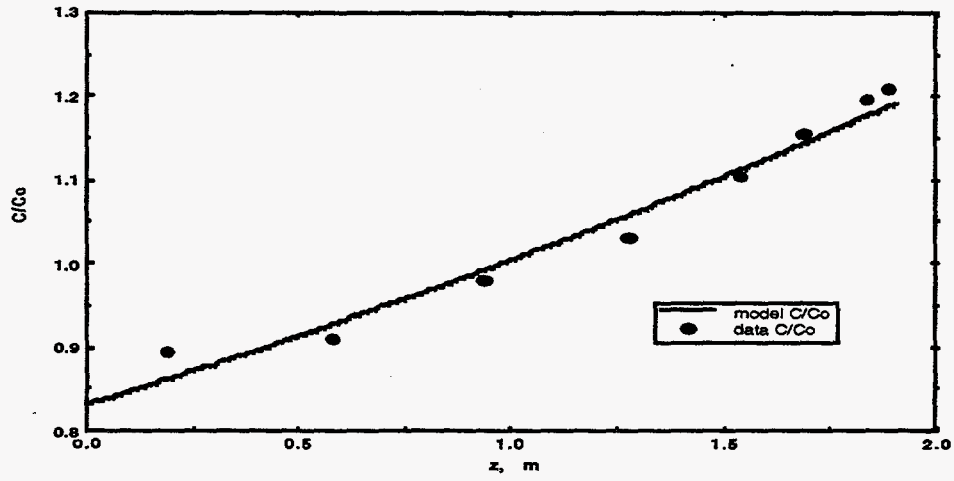

Figure 2. Steady-state concentration profile of kaolinite clay particles in the bubble fraction column.

4.2 Formation and Properties of Surfactant-stabilized Microbubbles

Success of the proposed remediation approach is based on the formation and stability of gas microbubbles. The lifespan of air microbubbles in pure water is relatively short. However, if the microbubbles are coated with surface-active agents (surfactants), the surfactant molecules will reduce gas diffusion from the bubbles toward the liquid phase and will also reduce coalescence among bubbles.

Surfactant-coated microbubbles were generated using a sonicator or a spinning disk. The microbubbles produced with the sonicator are fairly monodispersed with a diameter smaller than 1-2 μm (measured using a Coulter Multisizer II). The typical bubble concentration ranged from 5 x 10^7 to 9 x 10^7 mL-1. Larger volumes (1500 mL vs. 60 mL with the sonicator) and greater concentrations of bubbles (up to 2.3 x 10^8 mL-1) were prepared using the spinning disk. With this technique, however, two sizes are generated: microbubbles smaller than 3 μm and microbubbles ranging from 3 to 15 μm (Figure 3). The finer bubbles account for approximately 70 - 80% of the total bubble population.

The surfactants used to stabilize the microbubbles included nonionic surfactants (Tween 80, Triton X100, Span 60, and Span 40), anionic surfactants (sodium dodecyl sulfate or SDS, and sodium dodecyl benzene sulfonate), and a cationic surfactant (cetyltrimethyl ammonium bromide or CTAB). A single surfactant alone did not stabilize the gas microbubbles. In fact, as previously reported by Wheatley and Singhal (1995), one of the Span surfactants had to be present to stabilize the bubbles. Mixtures typically studied are SDS/Span 60, Tween 80/Span 60, SDS/Tween 80/Span 60, and CTAB/Span 60.

Stability of the bubbles is currently being determined as a function of surfactant type and concentration. Preliminary results have indicated that after an initial drop in microbubble concentration, bubbles remain stable for several weeks in the surfactant solution. Dilution experiments have shown that the bubbles are stable for up to six days. Experiments are underway to study the effects of ionic strength and hardness on the stability and size of the microbubbles. Additional experiments have also begun to determine the bubble surface charge using a Coulter DELSA 400SX.

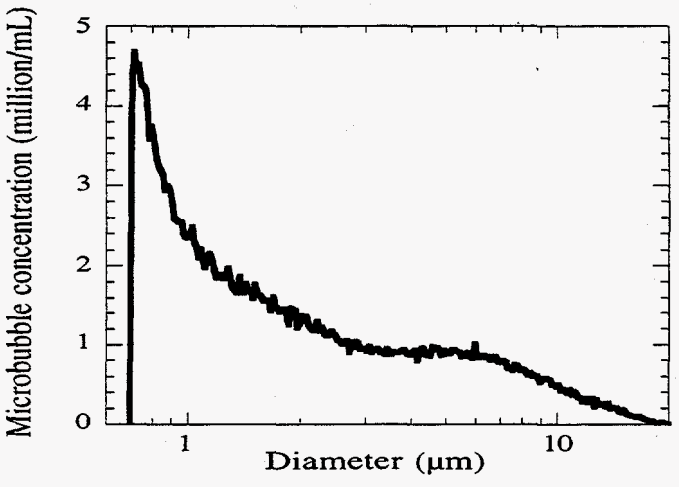

Figure 3. Concentration and size distribution of microbubbles obtained using the spinning disk. Surfactants: SDS and Span 60.

4.3 Microbubble Transport in Porous Media

The mobility and stability of microbubbles in saturated subsurface environments needs to be understood as part of the feasibility evaluation of the proposed remediation technique. In

particular, the microbubble-based remediation approach requires the capability of efficient microbubble transport without significant decay. Transport is diminished by microbubble sorption onto mineral surfaces, while decay results from microbubble gas dissolution as well as coalescence into larger bubbles. Growth of larger bubbles at the expense of microbubbles is unfavorable because this results in a practically immobile distribution of gas bubbles (strained within finer pores) and lower available interfacial area for contaminant sorption. In this section, we show how the main features of microbubble transport in groundwater can be characterized in the context of filtration theory. We then provide brief descriptions of our initial laboratory column studies on microbubble transport and upcoming experiments.

Studies of colloid transport in groundwaters borrow heavily from filtration theory (Tien and Payatakes, 1979). Since microbubbles are surfactant-encapsulated gas bubbles in the colloid size range (~10^{-8} to 10^{-6} m), we hypothesize that their transport in groundwater can be approximated by the colloid advection-dispersion equation, suitably modified to account for microbubble properties. Analyses of long-term transport requires consideration of microbubble dissolution as well as coalescence, sorption onto mineral surfaces, and buoyant rise. These last two factors dominate short-term transport of stable microbubbles, and relate to microbubble surface charge, size, mass density and interfacial mobility. Microbubble surface charge characteristics are expected to be surfactant- and solution-dependent, and will be quantified in upcoming studies. The buoyant rise of microbubbles is described by Stokes law. Modification of Stokes law to accommodate interfacial mobility and microbubble gas phase circulation is expected to be minor because of surfactant-encapsulation (Landau and Lifshitz, 1987). Buoyancy results in two main effects: microbubble rise relative to water, and (given attractive interactions) microbubble sorption on mineral grains. Note that buoyancy-initiated microbubble sorption at mineral surfaces is directly analogous to sedimentation-initiated colloid filtration, a process that has been extensively characterized in filtration theory. When collector-particle (sand-colloid) interactions are attractive, collection (sorption) efficiency depends strongly on the gravitational group, the ratio of sedimentation velocity to average pore fluid velocity. The fact that microbubbles in the 0.5 to 1 μm size range have buoyant rise velocities (in water) in the range of 10 to 50 mm d^{-1}, much slower than typical groundwater velocities, indicates that microbubble immobilization on aquifer grain surfaces may be minor. This is favorable for purposes of dispersing microbubbles over large volumes of contaminated groundwaters. However, it should be noted that groundwater flows are typically nearly horizontal, transverse to the vertically directed rise of microbubbles. All filtration studies of sedimentation effects have been conducted with vertical flow of suspensions. Our initial microbubble transport experiments are also conducted with vertical flow, in order to borrow from and build upon the wealth of existing research. At the end of this section, we briefly describe plans for near-future microbubble transport experiments in horizontal flow fields more typical of groundwater systems.

Our initial microbubble transport experiments were conducted in short, vertical, sand columns, under hydrostatic and steady-state flow conditions. Well-washed Unimin sand (425-500 μm) was packed into 24 mm ID glass columns. The columns' lengths differed for the hydrostatic and flow experiments, and are specified later. The bulk density, porosity, and hydraulic conductivity of these packings were 1.70 Mg/m^{-3}, 0.36, and 7.1 x 10^{-4} m/s^{-1}, respectively.

Two hydrostatic microbubble transport experiments were performed, both in a 50-mm tall sand column. In the first experiment, a Span60/Tween80 microbubble suspension was prepared. It had a microbubble concentration of about 10^{8} mL^{-1} in the 1 ± 0.5 μm size range. In the second experiment, a Span60/SDS microbubble suspension was used. Experiments were initiated by injecting a microbubble suspension into a 19 mm deep reservoir at the bottom end of a water-saturated sand column. The upper end of the column was connected to a hydrostatic pool of water that was periodically sampled for microbubble breakthrough. No microbubble breakthrough was observed in either experiment, even after a period of four times the free rise travel time. These

results indicate that sorption onto sand surfaces strongly retards microbubble transport under hydrostatic conditions.

Two microbubble transport experiments have been completed in 200 mm tall sand columns. In addition to the previously mentioned column properties, a dispersivity of 1 mm was determined in a separate NaCl breakthrough curve measurement. Span60/SDS microbubble suspensions were used for the transport tests, with concentrations in the range of 10^8 mL^{-1}, primarily in the 0.6 - 1.0 μm size range. For each experiment, one pore volume of this microbubble suspension was injected into the bottom of the water-saturated sand column, followed by further infusion with water. Flow was controlled by a syringe pump, with effluent diverted into a fraction collector. The microbubble suspension in the syringe was periodically agitated via a small enclosed magnetic stir-bar in order to maintain nearly constant inflow suspension concentrations. The two experiments were conducted at average pore water velocities of 6.0 and 0.6 m d^{-1}, corresponding to gravitational group numbers of 8 x 10^{-3} and 8 x 10^{-2}, respectively. Microbubble breakthrough curves were fit by an analytical solution to advective-dispersive transport with reversible sorption (van Genuchten and Alves, 1982). Breakthrough curve results (Figure 4) show essentially conservative microbubble transport with some sorption-induced retardation. These results are encouraging since they indicate that microbubbles can be effectively transported under both slow and typical groundwater velocities.

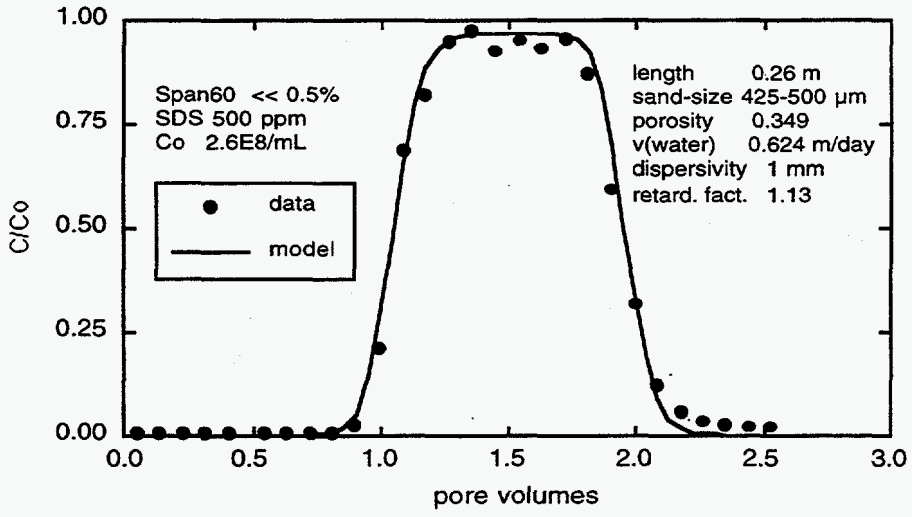

Figure 4. Breakthrough curve for Span60/SDS microbubbles transported through a sand column at low flow rate (pore water velocity = 0.624 m/day).

Upcoming studies on microbubble transport will focus on three areas. First, experiments in finer sands will be tested to determine grain-size limitations for microbubble transport. Second, microbubble transport experiments in 2-D sand packs under horizontal flow will be performed to determine the influence of flow transverse to the direction of buoyant rise. As noted previously, this is important since groundwater movement is typically nearly horizontal. Third, microscopic visualization of microbubble transport will be conducted in vertically oriented glass micromodels (Wan et al., 1996), under both horizontal and vertical flows. These visualization studies will help in developing a mechanistic understanding of microbubble transport in porous media.

ACKNOWLEDGMENTS

We thank Mark Yahnke for technical support during the initial phase of this work.

5.0 REFERENCES

Landau, L.D., and E.M. Lifshitz,1987. Fluid Mechanics, 2nd. Ed. Oxford Pergamon Press.

Lemlich, R., 1966. A theoretical approach to nonfoaming adsorptive bubble fractionation. A.I.Ch.E.J., 12, 802-804.

Shah, G. N., and R. Lemlich, 1970. Separation of dyes in nonfoaming adsorptive bubble columns. Ind. Eng. Chem. Fundam., 9, 350-355.

Tien C., and A.C. Payatakes, 1979. Advances in deep bed filtration, A.I.Ch.E.J., 25, 737-759.

van Genuchten, M.Th., and W.J. Alves, 1982. Analytical solutions of the one-dimensional convective-dispersive solute transport equation. U.S. Dept. Agric., Tech. Bull. No. 1661, 151 p.

Wan, J. and J.L. Wilson, 1994. Visualization of the role of the gas - water interface on the fate and transport of colloids in porous media, Water Resour. Res., 30, 11-23.

Wan, J., T.K. Tokunaga, C.F. Tsang, and G.S. Bodvarsson, 1996. Improved glass micromodel methods for studies of flow and transport in fractured porous media, Water Resour. Res., 32, 1955-1964.

Wheatley, M.A., and S. Singhal, 1995. Structural studies on stabilized microbubbles: Development of a novel contrast agent for diagnostic ultrasound, reactive polymers, Reactive Polymers, 25, 157-166.

Rapid Mass Spectrometric DNA Diagnostics for Assessing Microbial Community Activity During Bioremediation

W. Henry Benner, Principal Investigator

Tel: 510/486-7194, Fax: 510/486- 5857, email: WHBenner@lbl.gov
Lawrence Berkeley National Laboratory
Mail Stop 70A-3363

Co-Investigator: J. Hunter-Cevera, (LBNL)

EXECUTIVE SUMMARY

The effort of the past year's activities, which covers the first year of the project, was directed at developing DNA-based diagnostic procedures for implementation in high through-put analytical instrumentation. The diagnostic procedures under evaluation are designed to identify specific genes in soil microorganisms that code for pollutant-degrading enzymes. Current DNA-based diagnostic procedures, such as the ligase chain reaction (LCR) and the polymerase chain reaction (PCR), rely on gel electrophoresis as a way to score a diagnostic test. We are attempting to implement time-of-flight (TOF) mass spectrometry as a replacement for gel separations because of TOF's speed advantage and potential for sample automation. We anticipate that if TOF techniques can be implemented in the procedures, then a very large number of microorganisms and soil samples can be screened for the presence of specific pollutant-degrading genes.

1.0 OBJECTIVE

The use of DNA-based procedures for the detection of biodegrading organisms or genes that code for pollutant-degrading enzymes constitutes a critical technology for following biochemical transformation and substantiating the impact of bioremediation. DNA-based technology has been demonstrated to be a sensitive technique for tracking micro-organism activity at the molecular level. These procedures can be tuned to identify groups of organisms, specific organisms, and activity at the molecular level. We are developing a monitoring strategy that relies on the combined use of DNA diagnostics with mass spectrometry as the detection scheme. The intent of this work is a two-fold evaluation of 1) the feasibility of replacing the use of gel separations for identifying polymerase chain reaction (PCR) products with a rapid and automatable form of electrospray mass spectrometry and 2) the use of matrix-assisted-laser-desorption-ionization mass spectrometry (MALDI-MS) as a tool to score oligonucleotide ligation assays (OLA).

2.0 APPROACH

We have chosen to investigate TOF procedures that detect 1) when two approximately 20-base long oligonucleotides are ligated, 2) PCR products in the 100 bp (base pair) size range, 3) PCR products in the megadalton size range, i.e., ≥ 1500 bp and 4) plasmids that carry catabolic genes. This course of investigation is based on performance characteristics of current mass spectrometry capabilities under development in our laboratory. We began by developing the necessary molecular biology procedures and then started to evaluate the use of matrix-assisted-laser-desorption-ionization time-of-flight mass spectrometry (MALDI-TOF-MS) and charge detection mass spectrometry (CDMS) as detection schemes[1, 2].

The naphthalene enzymatic-degradation pathway is shown in the schematic[3] in Figure 1, and capital letters refer to the various steps in the pathway. We have focused on steps C and H that occur as a result of the activity of the nahC (1,2 dihydroxynaphthalene oxygenase) and nahH (catechol oxygenase) enzymes, respectively.

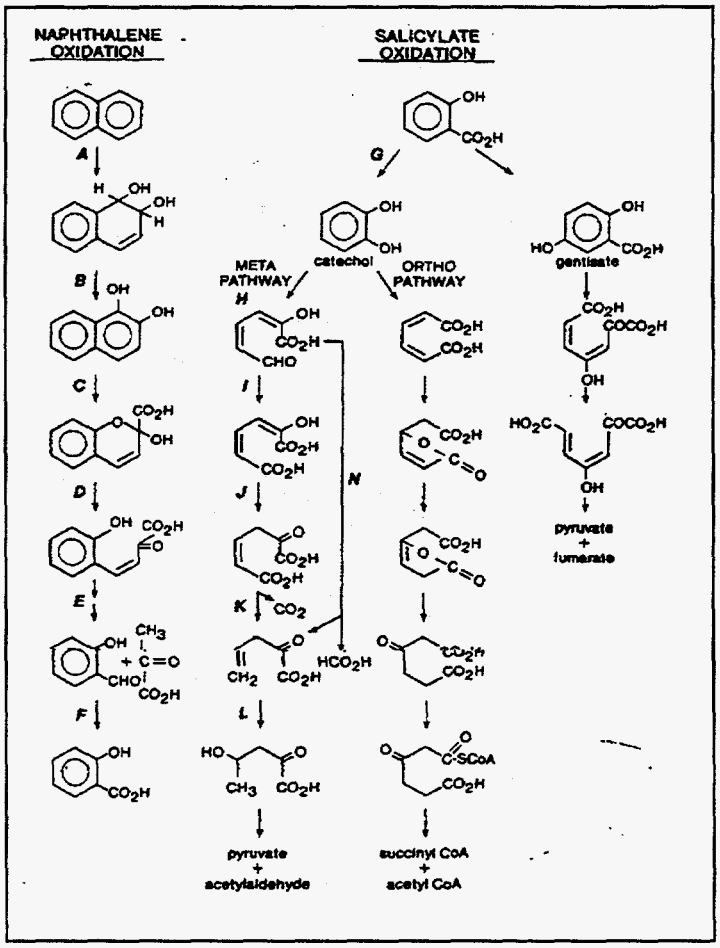

Figure 1. Naphthalene degradation pathway

Pseudomonas stutzeri P-16, an organism observed by W. Stringfellow, Center for Environmental Biotechnology, LBNL, to grow using naphthalene as its only carbon source was selected as a source of DNA for testing our proposed diagnostic procedure. A GenBank search for genes coding for nahH and nahC revealed that several highly similar sequences are shared by a few strains of *Pseudomonas*. Regions of high sequence similarity in nahH and nahC were used to direct the design of primers for the LCR. Genomic DNA was isolated from *Pseudomonas stutzeri* P-16 and used as a target in an LCR assay. We were unable to obtain a positive LCR test even when 1008 degenerate primers were utilized in the assay to compensate for several uncertainties in the target sequence. The negative results were assumed to be caused by the sequence uncertainties and the resulting low concentrations of degenerate primers introduced into the reaction. Therefore, we attempted to sequence a short section of the nahH gene to confirm or disprove its presence in P-16, and if present, use the sequence to design unique primers. Primers were selected to amplify a 161-bp region and PCR generated the expected product. We observed that the sequence we determined is very similar, yet unique, to genes for catechol oxygenase.

Using the sequence obtained for the 161-bp region of the nahH gene, a new set of LCR oligonucleotides was selected and a series of reactions was run to optimize product amplification while simultaneously minimizing template-independent ligation. A colorimetric assay using an alkaline phosphatase labeled primer was used to analyze the results of the reactions. The following parameters were investigated: primer concentration, template concentration, non-homologous (salmon sperm) DNA concentration, ligase concentration, and thermal cycle number. The following parameters yielded the best ratio of positive amplification to negative control for a 50 µL reaction:

- Primer Concentration: 10 fmol/µL
- Template Concentration: 20 zmol/µL
- Salmon Sperm Amount: 250 ng
- Ligase Amount: 2 units
- Thermal Cycle Number: 32

With this set of primers and primer binding conditions we were able to detect the nahH gene in genomic DNA isolated from P-16 using a LCR diagnostic procedure. This establishes the completion of one milestone of the project, namely the demonstration of a test useful for detecting a specific gene in a pollutant-degrading organism. We are currently working to establish an appropriate magnetic bead-based affinity capture technique for use in concentrating and desalting the ligated product so that it can be identified by MALDI-TOF-MS.

In an attempt to evaluate the possible application of CDMS as a tool for detecting large PCR products, we generated a 1982 bp long strand using pUC19 as template DNA. This template was chosen because the conditions and primers were readily available and thus

provided a quick way to test the capability of CDMS in this particular application. In the CDMS technique, electrospray converts DNA molecules in solution into highly charged gas-borne DNA ions. The ions are then directed to fly through a Faraday tube where their image charge signal is measured. This leads to a mass measurement of individual ions. When applied to PCR products in the megadalton size range, a mass measurement provides a way to determine the size of the DNA strand. Mass measurements can be acquired from as few as about 1000 ions in a time period as short as about 10 min. When this procedure is compared to the several hours of time needed to separate the PCR product on an electrophoresis gel, the time saving is obvious. Figure 2 shows a mass spectrum of the 1982 bp PCR product determined with the CDMS technique.

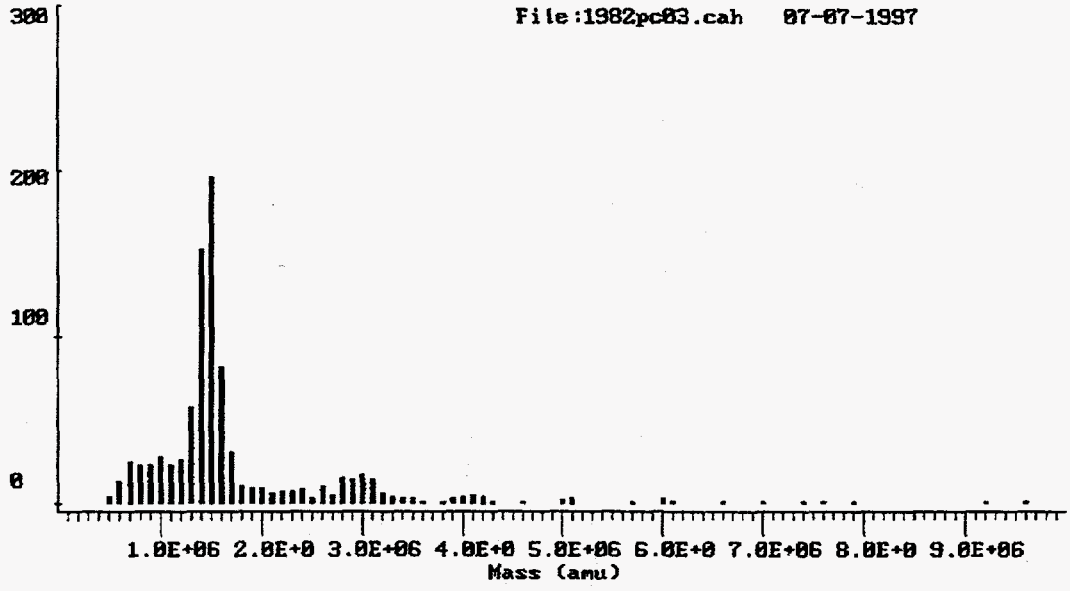

Figure 2. Mass spectrum of a 1982 bp (1.3 MDa) PCR product.

The assay that we are developing is specific to naphthalene and can be used to track the bioremediation of naphthalene. Future work will be directed towards transforming this technique into a more general procedure so that it could be applied to the investigation of other pollutants and their degradation pathways.

---

[1]Fuerstenau, S.D. and W.H. Benner, Molecular Weight Determination of Megadalton DNA Electrospray Ions Using Charge Detection Time-of-Flight Mass Spectrometry, Rapid Commun. Mass Spectrom., 9, 1528-1538, 1995.

[2] Schultz, J.C., C. A. Hack and W.H. Benner, Mass Determination of Megadalton-DNA Electrospray Ions using Charge Detection Mass Spectrometry, submitted to J. Am. Soc. Mass. Spec., 1997.

[3] Yen, K.-M. and C. M. Serdar, Genetics of Naphthalene Catabolism in Pseudomonas, CRC Critical Rev. in Microbiol., 15, 247-263 , 1988.

Enzyme Engineering for Biodegradation of Chlorinated Organic Pollutants

Principal Investigator:
Peter G. Schultz, Tel: 510/495-9277, Fax: 510/486-6890, email: pgschultz@lbl.gov
Lawrence Berkeley National Laboratory
Mail Stop: UCB, Latimer

1.0 OBJECTIVES

The focus of our program is the development of tailor-made biological catalysts for modifying or degrading halogenated compounds and other environmental pollutants. Our approach takes advantage of the tremendous chemical diversity of antibodies. Recently, this diversity and specificity have been merged with our understanding of chemical reactivity to generate a new class of antibody molecules-catalytic antibodies. This new technology makes possible the generation of antibody molecules that not only *selectively bind*, but that also *chemically transform* virtually any molecule of interest. Because antibodies can be elicited to a huge array of biopolymers, natural products, or synthetic molecules, catalytic antibodies offer a unique approach for generating tailor-made enzyme-like catalysts with a desired selectivity. At the same time, the characterization of catalytic antibodies provides fundamental state stabilization, proximity effects, general acid and base catalysts, and electrophilic and nucleophilic catalysis and strain.

2.0 APPROACH

Our initial goal is to develop powerful new methods for screening or selecting catalytic antibodies from large antibody libraries. We are using as a model system the catalytic antibody 43C9, which hydrolyzes aryl amides. We have cloned and expressed this antibody under the arabinose promoter as a chimeric Fab. Induction leads to the expression of 10 to 100 mM levels of antibody in the periplasm. An amide derivative of p-aminobenzoic acid (PABA) has been synthesized. Hydrolysis of the amide bond by antibody 43C9 will lead to the release of PABA that will complement an aro C^- *E. coli* auxotroph. Mutants of 43C9 generated by *in vitro* mutagenesis methods can then be selected based on this growth selection. The requisite aro C^- mutant has been generated and background growth rates on PABA and the amide derivative have been measured. We are currently generating libraries of variable region mutants by DNA shuffling. We are also synthesizing an amide derivative of the substrate that when hydrolyzed will release indigo, providing a chromogenic assay of catalytic activity that can be used in a plate screen of libraries of mutants.

If these experiments are successful they will provide a general strategy for evolving protein catalysts with a broad range of specificities and activities. We then will directly apply these approaches to the generation of antibodies that catalyze the hydrolysis of halogenated aromatics. In this case we will use an antibody that binds halogenated nitrobenzene but that currently lacks hydrolytic activity (such an antibody is in hand). We will generate libraries of variable region mutants and select or screen for those with hydrolytic activity using the approaches described above.

Evaluation of Isotopic Diagnostics for Subsurface Characterization and Monitoring: Field Experiments at the TAN and RWMC (SDA) Sites, INEEL

Principal Investigators:
Donald J. DePaolo Tel: 510/495-2228, Fax: 510/486-5686, email: djdepaolo@lbl.gov
B. Mack Kennedy, Tel: 510/495-6451, Fax: 510/486-5686, email: bmkennedy@lbl.gov
Lawrence Berkeley National Laboratory

Co-Investigators: Mark Conrad (LBNL)
Eric Miller and Thomas Wood (INEEL)

1.0 INTRODUCTION

This research is aimed at improving methods for characterizing underground contamination sites and for monitoring how they change with time. Particular emphasis is placed on identifying and quantifying the effects of intrinsic remediation and verifying the efficacy of engineered remediation activities.

Isotopic measurements of elements such as C, O, H, He, Cl, and Sr, which are present in groundwater and soil gas, provide a quantitative measure of material balance. They can be used to identify the sites of origin of contaminants in groundwater, and to determine if contaminants are being destroyed as a result of natural processes or engineered processes. Isotope ratios also can be used to trace the migration of fluids that are pumped down wells to destroy or confine underground contaminants, such as steam and grout, and they can be utilized to diagnose what chemical reactions are occurring underground and what materials are reacting. For example, destruction of TCE usually produces carbon dioxide, but carbon dioxide can also come from dissolution of calcite.

There are many isotopic ratios that can be measured in groundwater and vadose zone gas that could be valuable for characterizing remediation sites and monitoring remediation activities. We concentrate on a few that are particularly useful for the problems being addressed at the TAN (Test Area North) and RWMC (Radioactive Waste Management Complex) sites of the Idaho National Engineering and Environmental Laboratory. The isotopes we are using are ^{13}C, ^{14}C, ^{3}He, ^{87}Sr, ^{37}Cl, and ^{18}O.

2.0 DESCRIPTION OF FIELD SITES

2.1 The Test Area North (TAN) site

From 1955 to 1972 a variety of waste materials, including low-level radioactive isotopes, sewage, and chlorinated solvents, were disposed of in a 94.5 m well both above and below the water table. The resultant plume of TCE, DCE, ^{90}Sr, ^{137}Cs, ^{3}H, and some other contaminants in the Snake River aquifer, is moving southeastward at the rate of about 100 m/yr. The plume, which is mapped using TCE concentrations (Figure 1), extends about 2 km downstream from the source.

The plume appears to be restricted at present in the vertical dimension between the water table (60 m depth) and 120 m depth, due to the presence of an impermeable layer at ca. 120 m depth, although there is some indication that the plume has broken through this layer to deeper levels in at least one place. The primary remediation issue here is the TCE contamination of the aquifer water. The radionuclides are of secondary concern, partly because they appear to be strongly retarded in the plume. The regulatory goals are to eliminate the source of the contamination, defined as the 5000 µg/l concentration isograd of TCE, and to decrease the remaining contamination to below the MCL for TCE (5µg/l). The present remediation work is by pumping and treating. However, because TCE is relatively insoluble, the rate of removal of TCE from the ground is small. Removal of the contamination source will probably entail extraction or *in situ* destruction of TCE by some form of oxidation. Reduction of the plume TCE concentration to below MCL may also require some form of *in situ* destruction of TCE unless natural attenuation is shown to be sufficient.

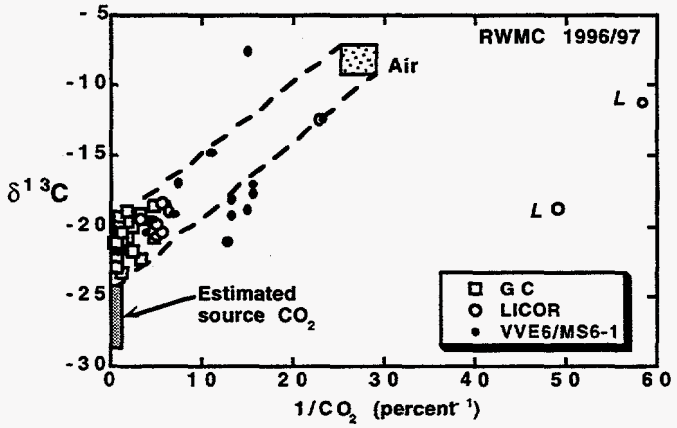

Figure 1. Relationship between the CO_2 concentration and the $^{13}C/^{12}C$ ratio of the CO_2 in subsurface gas at RWMC; the $^{13}C/^{12}C$ ratio is expressed as $\delta^{13}C$. The samples with the highest CO_2 concentrations have the lowest $\delta^{13}C$, indicating that the CO_2 is being produced by oxidation of organic carbon. The $\delta^{13}C$ corresponding to the intercept $(CO_2)^{-1} = 0$ is normally about 4 permil higher than the $\delta^{13}C$ of the source carbon (Cerling et al., GCA 55, 3403, 1991), so the carbon source probably has $\delta^{13}C$ slightly below -25. This value corresponds closely to that of typical lubricating oils buried at the site, but not to chlorinated solvents, which normally have lower $\delta^{13}C$ values of -23 to -50. Data labelled "L" are examples of sampling artifacts caused by leakage of the sample bags during shipping. There is a suggestion that the CO_2 in the background wells (VVE-6, M6S) is partly from a source with lower $\delta^{13}C$.

2.2 Subsurface disposal area (SDA) of the Radioactive Waste Management Complex (RWMC)

Volatile organic compound (VOC) contaminants are present in the vadose zone beneath and within the immediate vicinity of the Subsurface Disposal Area (SDA) of the Radioactive Waste Management Complex (RWMC) (see Figures 2, 3, and 4). Depth to the water table is greater than 150 m, with perched water above sedimentary interbeds. The source of contamination is 332,640 liters of organic waste disposed of in various pits and trenches in the SDA from 1966 to 1970. Wastes in pits include drums with mixtures of chlorinated solvents (CCl_4, TCA, PCE, TCE) and lubricating oil. Leakage from the drums has resulted in a plume of contaminants and possible

metabolic byproducts (e.g., chloroform, vinyl chloride) in the vadose zone. It is believed that the VOCs are mainly in rubble zones and highly permeable fractures in the basalt host.

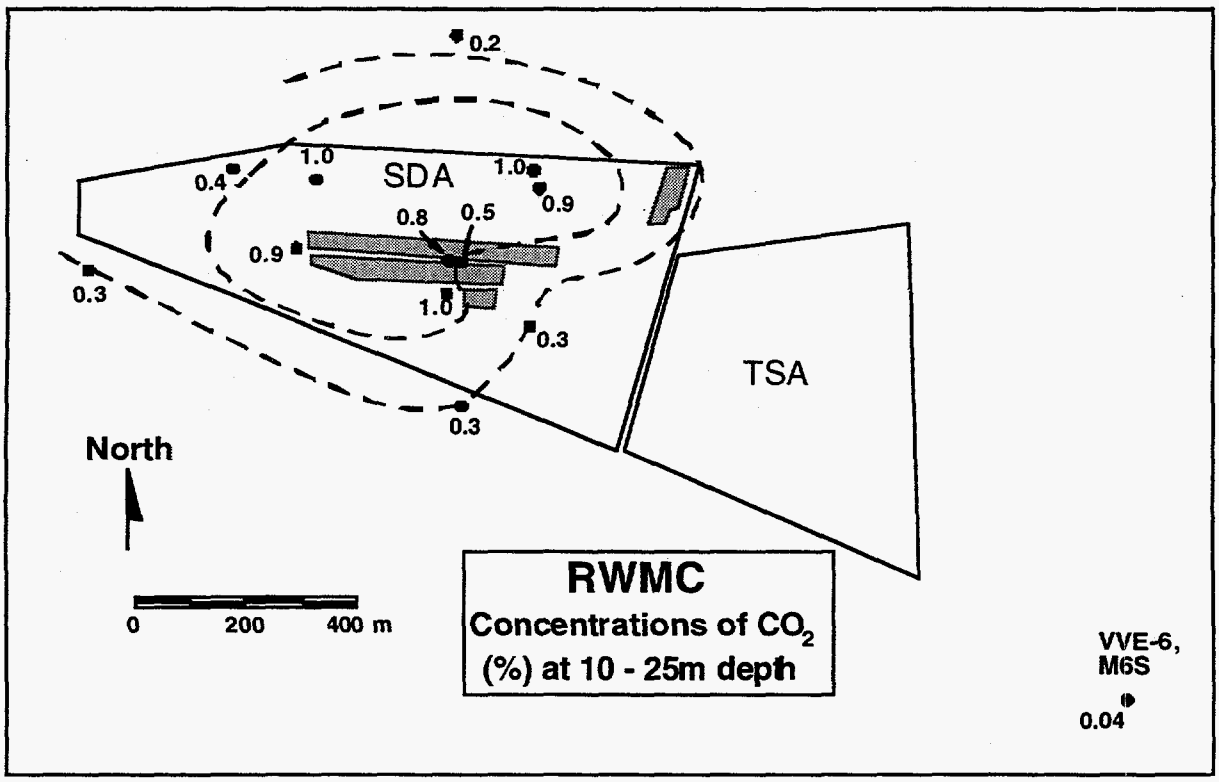

Figure 2. Map of the Radioactive Waste Management Complex at INEEL, showing locations of wells where gas samples were obtained for isotopic analysis during the period November 1996-June 1997. Numbers shown are concentrations of CO_2 in percent; contours are shown at about 0.3 and 0.5%. The wells to the southeast (VVE-6 and M6S) were sampled to represent "background values." A CO_2 concentration of 1% is about 30 times the atmospheric value, and about 20 times the subsurface background value.

Present remedial activities use a vapor vacuum extraction (VVE) technique to withdraw the contaminants from the vadose zone so they can be treated and disposed of at the surface (Figures 3 and 4). Successful remediation depends on understanding vapor flow in the vadose zone. High permeability features may act as preferential fast flow paths that affect the efficiency of the VVE process. Other issues concern whether VOCs are being continually released as they are being pumped out, at what rate, and whether the VOCs are being naturally remediated by biological activity or other types of reactions.

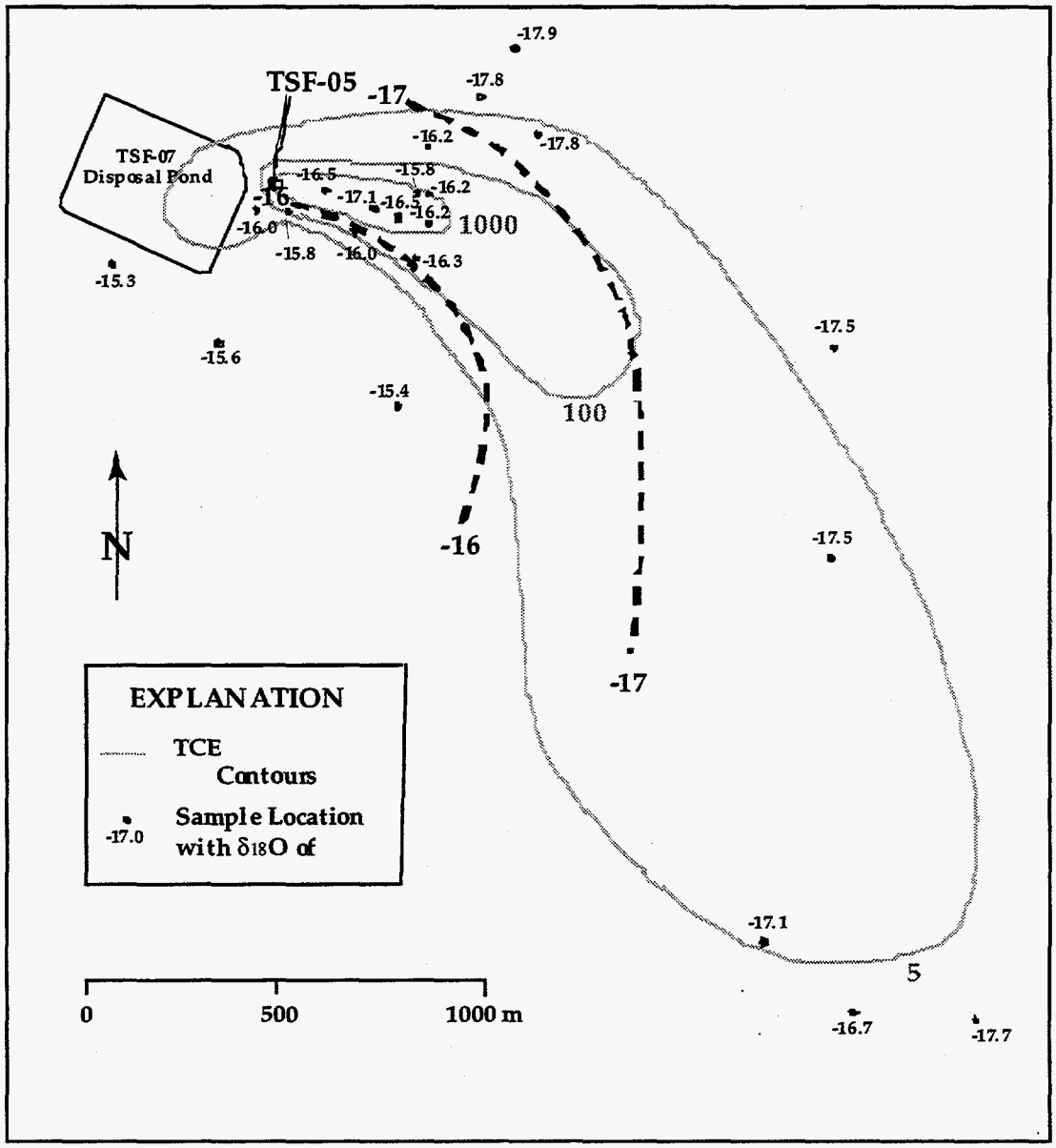

Figure 3. Map of the Test Area North (TAN) site at INEEL, showing TCE plume and $\delta^{18}O$ values of groundwaters sampled in summer 1997. The waters with $\delta^{18}O$ values greater than -16.5 show evidence of evaporation and may be affected by infiltration below the TSF-07 disposal pond. The waters with high $\delta^{18}O$ also have low $\delta^{13}C$ in dissolved inorganic carbon, an effect that may be indicative of active biodegradation of organic material.

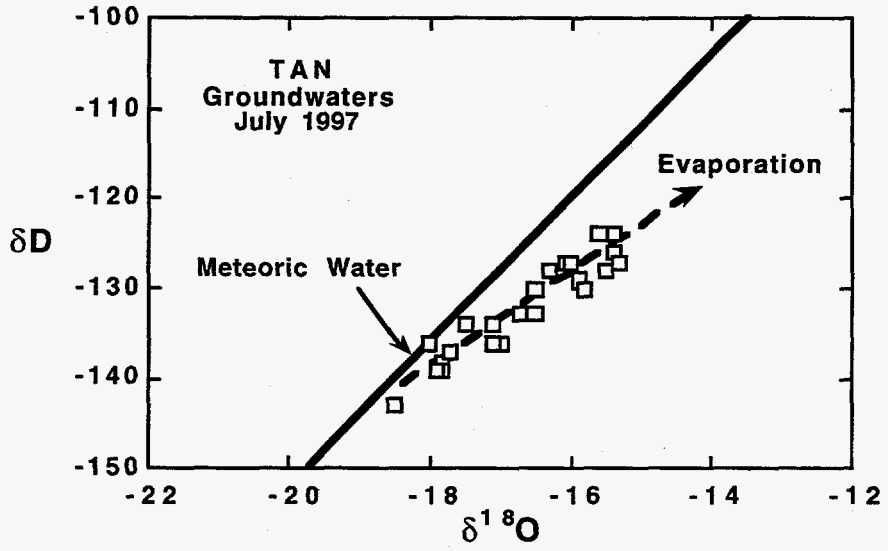

Figure 4. The $\delta^{18}O$ and δD values of TAN groundwaters indicate that they contain a component of water that has been affected by evaporation. Evaporation causes there to be a different relationship between $\delta^{18}O$ and δD than observed for normal meteoric waters.

3.0 SAMPLING

Application of the isotopic techniques requires field sampling and the return of the samples to the laboratory for analysis. At RWMC, vadose zone gas samples are obtained routinely for monitoring of CCl_4 and other contaminants. The sampling is done via a series of monitoring wells that surround the site of the buried materials. Wells located relatively far from the burial trenches penetrate to the water table whereas those close to the burial trenches penetrate to about 61 m in depth.

The character of subsurface gas at RWMC varies seasonally and with the operation of the VVE system, so it is necessary to sample the system relatively often to characterize it. A subset of samples from the normal weekly monitoring of RWMC was sent to us at LBNL in November 1996, February 1997, March 1997, and June 1997. The sampling is continuing. A set of water samples from TAN groundwater was sent to us in July of 1997. The TAN groundwater plume evolves on a much slower time scale than the RWMC vadose zone plume, so sampling needs to be done only a few times during the course of the study.

4.0 MEASUREMENTS

The RWMC gas samples have been measured for $^{13}C/^{12}C$ ratios, $^{14}C/^{12}C$ ratios, and the concentrations of CO_2, O_2, and N_2. Noble gas concentration and isotopic analyses are planned but have not yet been carried out. TAN water samples have so far been measured for $^{13}C/^{12}C$ ratios, $^{18}O/^{16}O$ ratios, D/H ratios and the concentration of dissolved inorganic carbon (DIC). Measurements of $^{87}Sr/^{86}Sr$ and $^{14}C/^{12}C$ ratios of TAN waters are underway.

5.0 RESULTS

- There is substantial production of CO_2 in the subsurface of the RWMC site. This production is far above the background values that can be observed outside from the Subsurface Disposal Area (SDA; Figure 2). The vadose zone CO_2 has a low $^{13}C/^{12}C$ ratio and therefore appears to be an oxidation product of organic material (Figure 2). It is not yet possible to determine with confidence which organic material is being oxidized and by what mechanism, but our preliminary assessment is that the source of the CO_2 is oxidation of the lubricating oil rather than oxidation of the chlorinated solvents.

- Initial ^{14}C analyses of the CO_2 indicate the presence of an additional, radioactive source for the CO_2 in the vadose zone of RWMC. This source is tentatively identified as buried reflector blocks from nuclear reactors. Evidence of migration of the ^{14}C is found in the "background" monitoring well about 1 km southeast of the trenches.

- A map of the $\delta^{18}O$ and δD values of groundwater at TAN indicate a region near and to the south of the injection well that has relatively high $\delta^{18}O$ (Figure 3). These waters also have δD values that indicate they have been subject to evaporation (Figure 4). These isotopic data indicate a significant contribution of evaporated water, presumably from the TSF-07 disposal pond.

- The $\delta^{13}C$ values of TAN groundwater DIC are 2-3‰ lower in the vicinity of the plume, indicating a possible contribution from degradation of contaminants (Figure 5).

- Analysis of $\delta^{18}O$ and $\delta^{13}C$ in TAN groundwater from below the lower confining layer of the upper aquifer suggests that there is no exchange across the lower confining layer.

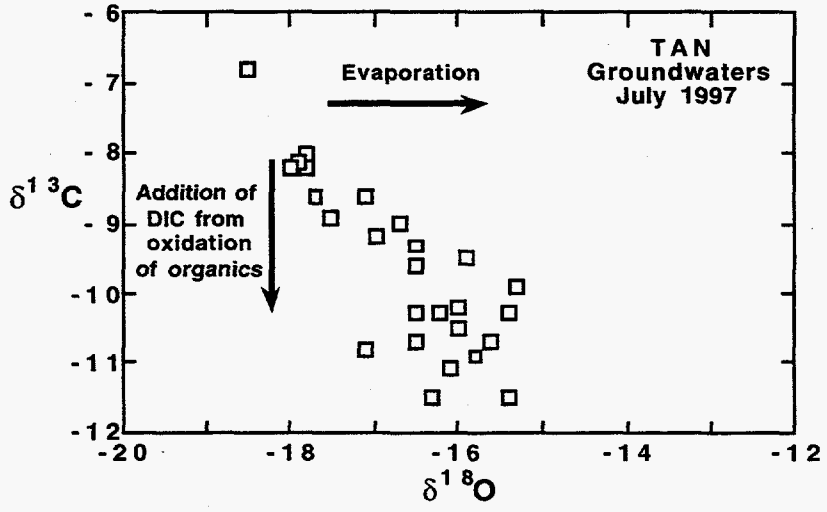

Figure 5. Relationship between carbon and oxygen isotopic composition in TAN waters. The low $\delta^{13}C$ values indicate a contribution to the dissolved carbon from oxidation of organic material, and this carbon is associated with the water that has been evaporated.

6.0 IMPLICATIONS

The preliminary results to date confirm that isotopic analysis of groundwaters and vadose zone gases are useful for diagnosing chemical processes occurring in the subsurface, and tracing the migration of waters from different sources. At both the RWMC and TAN sites there is evidence of biodegradation of organic material in the subsurface, although the evidence to date suggests that the most problematic contaminants are not being degraded at a significant rate. This needs to be confirmed with more analytical work and modelling.

A Chaotic-Dynamical Conceptual Model to Describe Fluid Flow and Contaminant Transport in a Fractured Vadose Zone

Principal Investigator:
Boris Faybishenko, Tel: 510/495-4852, Fax: 510/486-5686
email: bafaybishenko@lbl.gov

Lawrence Berkeley National Laboratory
Mail Stop 90-1116

Co-Investigators:
C. Doughty, J.T. Geller, S. Borglin, B.L. Cox, J.E. Peterson, Jr., M. Steiger, and K.H. Williams (LBNL)
T. Wood and R. Podgorney (Parson's Engineering Inc.)
T. Stoops (INEEL)
S. Wheatcraft, M. Dragila and J.C.S. Long (UNR)

ABSTRACT

Understanding subsurface flow and transport processes is critical for effective assessment, decision-making, and remediation activities for contaminated sites. However, for fluid flow and contaminant transport through fractured vadose zones, traditional hydrogeological approaches are often found to be inadequate. In this project, we examine flow and transport through a fractured vadose zone as a deterministic chaotic dynamical process, and develop a model of it in these terms. Initially, we examine separately the geometric model of fractured rock and the flow dynamics model needed to describe chaotic behavior. Ultimately we will put the geometry and flow dynamics together to develop a chaotic-dynamical model of flow and transport in a fractured vadose zone.

We investigate water flow and contaminant transport on several scales, ranging from small-scale laboratory experiments in fracture replicas and fractured cores, to field experiments conducted in a single exposed fracture at a basalt outcrop, and finally to a ponded infiltration test using a pond of 7 by 8 m. In the field experiments, we measure the time-variation of water flux, moisture content, and hydraulic head at various locations, as well as the total inflow rate to the subsurface. Such variations reflect the changes in the geometry and physics of water flow that display chaotic behavior, which we try to reconstruct using the data obtained.

In the analysis of experimental data, a chaotic model can be used to predict the long-term bounds on fluid flow and transport behavior, known as the attractor of the system, and to examine the limits of short-term predictability within these bounds. This approach is especially well suited to the need for short-term predictions to support remediation decisions and long-term bounding studies.

1.0 OBJECTIVES AND STRUCTURE OF THE PROJECT

Our primary objective is to determine when and if deterministic chaos theory is applicable to infiltration of fluid and contaminants through the vadose zone in fractured rock. To the extent that this theory is applicable we will develop algorithms for predicting flow and transport based on this theory.

In classical analysis, the system components are commonly taken to be cubes of equivalent porous media that tessellate the volume of interest. The rules used to describe multi-phase fluid flow are commonly given by Richard's Equation, a version of Darcy's Law, which describes how much fluid will be transferred as a function of the hydraulic head gradient and relative permeability.

For the case of infiltration in fractured rock, we will describe the geometry of the fracture network and determine the rules describing how fluid is transmitted as dynamical processes. The result of evaluating these processes will be an entirely new approach to the description of flow and transport behavior. The objectives of this project will be achieved through the development of:

- A hierarchical description of fracture geometry that controls fluid flow and transport,
- A dynamical description of infiltration and transport of contaminants in single fractures,
- An algorithm for flow and transport that combines the hierarchical geometry and the description of dynamical flow and transport,
- Appropriate techniques needed to detect chaotic behavior of flow in the field,
- Evaluation of deterministic chaos in laboratory and field experiments,
- Field investigations were conducted at the Box Canyon site in Idaho near the INEEL.

2.0 Background Information on Chaotic Dynamics and Fractal Structures

One of the central problems in the prediction of water, heat, and mass transfer in soils and fractured rocks is how to use past observations in order to predict the future. Field measurements can only employ a limited number of probes that cannot collect all needed information. Consequently, the quality of prediction using classical deterministic and stochastic differential equations with a set of initial and boundary conditions and volume-averaged parameters may be poor. One of the alternative approaches views a time series of data as a result of chaotic dynamics, which can appear even in a simple deterministic system. Random-looking data may in fact represent chaotic rather than stochastic processes. For predictive purposes, it is critical to recognize which is which, because for chaotic systems often only short-term predictions can be made. For example, it was shown that the weather predictability will approach zero for predictions of more than two weeks (Lorenz, 1982).

The differences between regular (non-chaotic deterministic), random, and chaotic systems are illustrated in Figure 2.1, which shows trajectories typical for each type of motion. Note that the flow trajectories for chaotic systems are different from both regular and stochastic systems. In general, the term chaotic process is used to describe a dynamical process with the following features: random processes are not a dominant part of the system, the trajectories describing the future states of the system are strongly dependent on initial conditions, adjacent trajectories diverge exponentially with time, the information on initial conditions cannot be recovered from later states of the system, and behavior is often characterized by an attractor that has a fractal geometry.

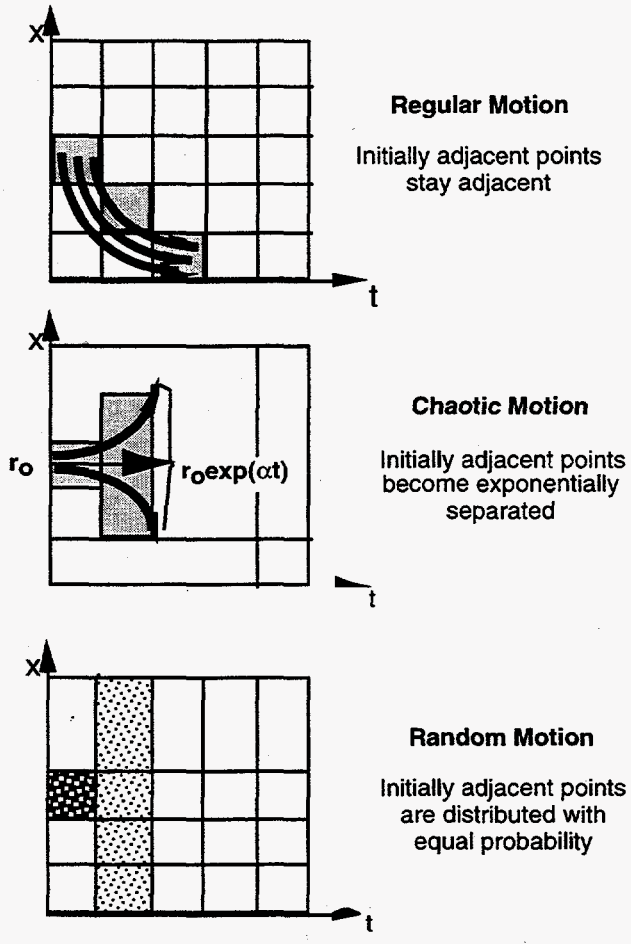

Figure 2.1 Comparison of regular (i.e., non-chaotic deterministic), chaotic, and random behavior (modified from Schuster, 1993).

Chaotic flow behavior in heterogeneous fractured media may result from hydrodynamic instabilities and a sensitive dependence of flow on (1) boundary conditions (precipitation, ambient temperature and pressure, groundwater fluctuations, etc.), (2) initial conditions (distribution of water content, pressure, and temperature), and (3) the current state of the system (water content, pressure, and temperature). Flow depends upon coupled effects of several non-linear factors such as the geometrical connectivity of the fracture system, air entrapment and its removal, clogging of the conductive fractures, biofilms, kinetics of the matrix-fracture water exchange, variability of effective hydraulic porosity and hydraulic permeability, and others.

The coupled effect of several non-linear processes in an unsaturated heterogeneous and fractured material causes non-linear behavior, governed by non-linear ordinary and partial differential equations, which may have bounded, nonperiodic solutions. These equations may be either: (1) purely deterministic where no random quantities appear in the equations (Moon, 1987; Tsonic, 1992), (2) chaotic-stochastic, or (3) have a noisy component (Kapitaniak, 1988). Therefore, one of the main problems in data analysis is to properly identify the type of the equation describing the flow system.

There are numerous examples of dynamical systems that display non-linear chaotic behavior for some system parameters. Some examples relevant to our study are: avalanche fluctuations

resulting from the perturbation of sandpiles of various sizes (Rosendahl et al., 1993), falling off of water droplets (Cheng et al., 1989), atmospheric temperature, river discharge, and precipitation (Pasternack, 1996; Pelletier, 1996), and oxygen isotope concentrations (Nicolis and Prigogine, 1989). One of the simplest examples is a dripping faucet (Shaw, 1984). Figure 2.2 shows a conceptual model of flow in fractured rocks based on a model of irregularly dripping water through a fracture, which produces non-periodic and non-repetitive behavior in both time and space.

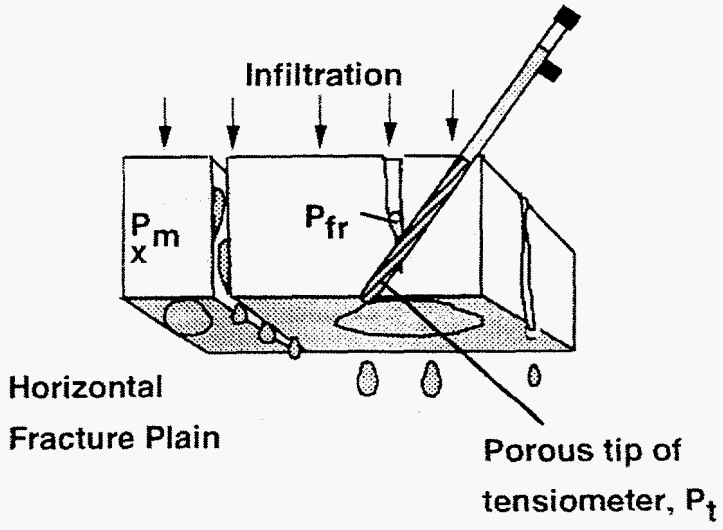

Figure 2.2 Conceptual model of flow and measurement in partially saturated fractured rocks. $P_x m$ = matrix water pressure; P_{fr} = fracture water pressure; P_t = tensiometer water pressure

It has been recognized that fractal structure is a possible indication of chaotic behavior of a system (Mandelbrot, 1977). Fractal analysis has been applied to many earth sciences problems, such as topography, fault traces, fracture networks, fracture surfaces, porous aggregate geometry, permeability distribution, flow and transport through heterogeneous media, erosion and chemical dissolution, etc. La Pointe (1988) used fractal geometry to characterize fracture density and connectivity. There are several papers in which the fractal properties of fractured tuff at Yucca Mountain were investigated (e.g., Carr, 1989). Fractal analysis was also used to predict bypass flow in rocks (Nolte et al., 1989; Cox and Wang, 1993) and clay soils with vertically continuous macropores (Hatano and Booltink, 1992).

3.0 Laboratory Tests (LBNL)

3.1 Introduction and Motivation

Observations of water seepage in fractures in the laboratory have shown the pervasiveness of highly localized and extremely non-uniform flow paths in the plane of the fracture (Geller et al., 1996). These channels exhibit intermittent flow behavior as portions undergo cycles of draining and filling, and small connecting threads snap and reform. This unsteady behavior occurs even in the presence of constant pressure boundary conditions. These observations motivated us to study dripping water between parallel plates as an idealized model of some of the flow behavior characteristic of water seepage through fractured rock. This study extends the classic chaos

experiment of the "dripping faucet" to drips in the presence of capillary forces as they are affected by the surface properties and the small aperture of the parallel plates.

The objective of these experiments is to collect data records that can be analyzed to determine whether or not, and under what conditions, the dripping of water in parallel plates is chaotic, random, or periodic. This work was further motivated by preliminary experiments that showed the sensitivity of pressure measurements to the formation and release of water drops through a needle in open air and inserted between parallel plates. Much of this year's work was invested in developing the experimental system to reliably obtain usable data records.

3.2 Experimental Results

Experiments were performed at a variety of flow rates to evaluate the system for chaotic behavior. Four basic types of experiments were conducted. Type A are pressure fluctuations caused by the 28 gauge needle dripping water into open air. Type B measure the baseline pressure fluctuations of the 28 gauge needle delivering water with a constant pressure condition at the needle outlet. (A constant pressure at the needle outlet was maintained by submerging the needle tip under water.) Type C use the 28 gauge needle to deliver water between smooth glass plates with a 0.35 mm gap at an angle of 60 degrees from the horizontal. Type D are identical to type C except for the use of rough glass plates. In each experiment, a constant flow rate of water was delivered as the magnitude of the pressure at the syringe needle was measured.

The smooth glass plates (type C) experiments were run at flow rates of 0.25, 0.5, 1.0, 1.5, 2.0, and 3.0 ml/hr. Typical pressure data for these flow rates are shown in Figure 3.1. In Figure 3.2 the frequency of drips and height of the average pressure fluctuation are plotted against the flow rates of the experiments in Figure 3.1. The experiments plotted in Figure 3.2 show a trend toward more frequent drip events and decreased height of pressure fluctuation as the flow rate increased. Visual observation of the drip events confirmed an increase in length of the thread of water as flow rate increased. However, duplicate experiments at each flow rate demonstrated that both the height of pressure fluctuations and the frequency of the drips vary between type C experiments with the same flow rate. The formation of the threads appear to depend qualitatively upon the initial condition of the plates. Some of the factors suspected to influence the drip frequency and length of thread formation are the amount of moisture on the plates, whether the drip was following a pre-existing flow path determined by a previous flow rate, and the cleanliness of the plates.

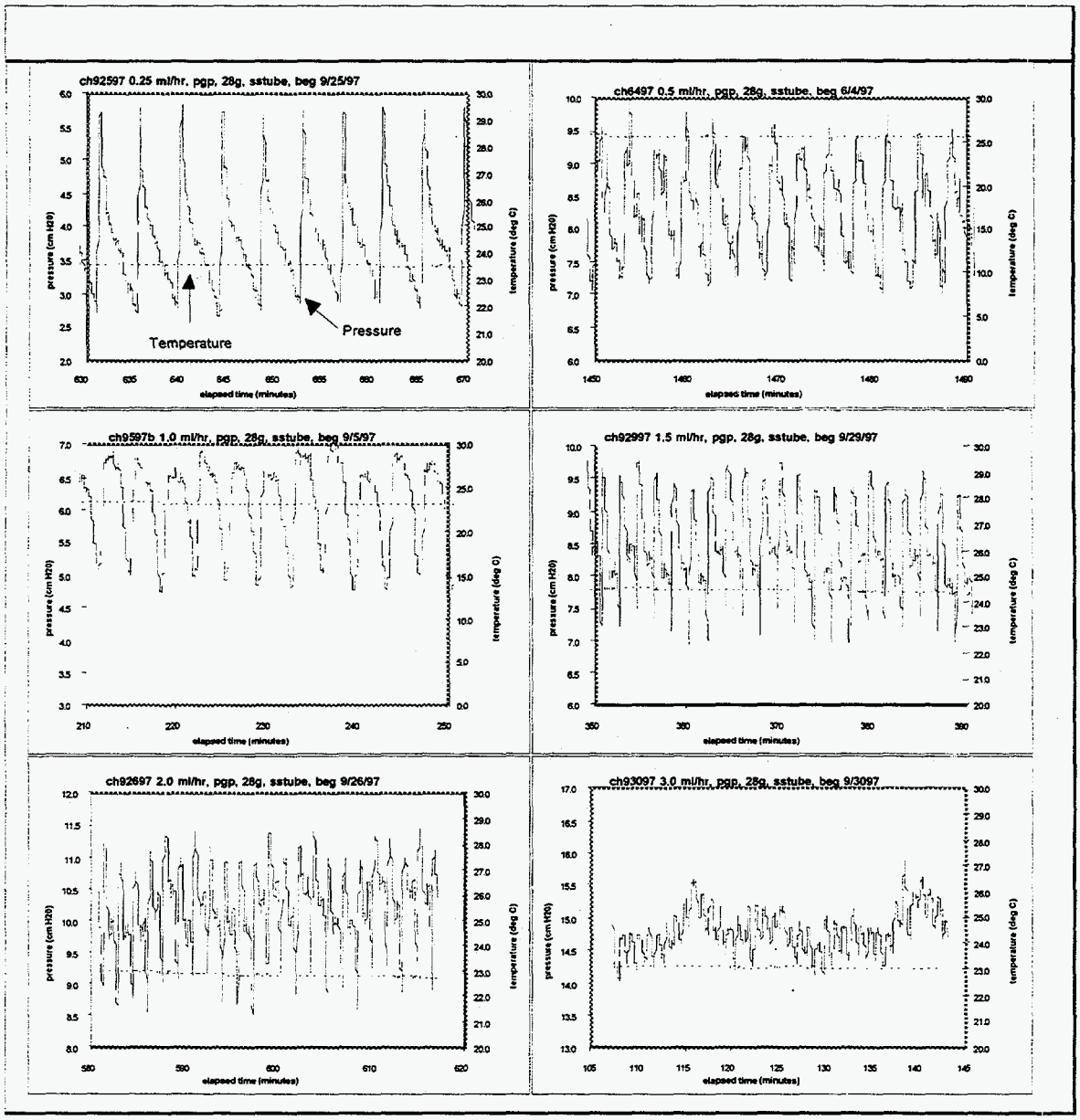

Figure 3.1: Smooth parallel glass plates. Pressure fluctuations caused by dripping water between smooth parallel glass plates at flow rates of 0.25, 0.5, 1.0, 1.5, 2.0, 3.0 ml/hr.

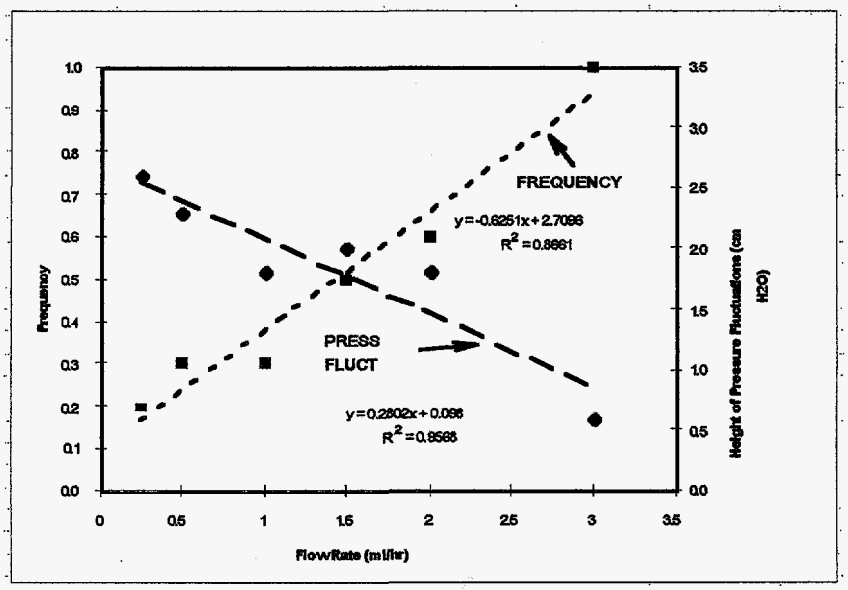

Figure 3.2: Observed trends in frequency and magnitude.

Experiments in roughened glass plates were conducted to test the effect of surface variability on drip behavior. Two types of plates were utilized: sand-blasted and shower-door glass (type D) plates. Both plates were separated by 0.35 mm shims. The sandblasted plates had an overall consistency of fine sandpaper with an even coating of fine (approximately 0.1 mm) irregularities on the surface. When the water was introduced into the sandblasted plates, a halo developed on the plate as the water advanced and film flow occurred, but drops did not form. The pressure signature observed from the sandblasted plates was similar to that observed for the baseline monitoring (see below).

The shower-door glass plates had larger, smooth irregularities or nubs on the surface (average scale of 2-3 mm). When the drips were introduced into the shower glass plates, the larger spaces between the nubs allowed drips to form at the end of the needle. The drops grew to different sizes before they snapped off and moved down the plate. Occasionally, short threads formed before the drop snapped off completely. After snapping off, the drop either moved quickly down the plate and was removed from the system or it remained close to the end of the needle, held back by a narrow throat formed by adjacent nubs. When the next drop formed, it tended to combine with the previous drop and the new larger drop would travel down between the plates.

The pressure fluctuation from the drips of water from the 28 gauge needle into open air (type A experiments) were recorded as a basis for comparison to the glass plate experiments. It was determined that the presence of capillary forces induced by the glass plates causes a decrease in drip frequency and a decrease in the height of the pressure fluctuation.

The experiments demonstrate the variation of observed pressure fluctuations and the importance of both identifying and controlling initial conditions to achieve consistent results. Although quantitative analysis of the results is not yet complete, these features suggest that chaotic dynamics play an important role.

4.0 Fractured Rock Outcrop Experiments (INEEL)

The outcrop scale experiments were designed and conceptualized to fill a gap of knowledge between the laboratory and field (Box Canyon, Idaho) scales of investigation. A research site was

selected at Hell's Half Acre Lava Field in Idaho where a single fracture could be studied. The site consisted of a basalt outcrop approximately 1 m thick that extended approximately 1.5 m outward from the rock wall. An infiltration gallery (0.5 x 1 m) was constructed above the fracture to perform constant head infiltration tests. On the underside of the overhang, drip sensors were installed to count and timestamp drops of water falling from the fracture. More traditional monitoring parameters, such as tension, temperature, and barometric pressure were also collected. Figure 4.1 shows the general site and instrument layout.

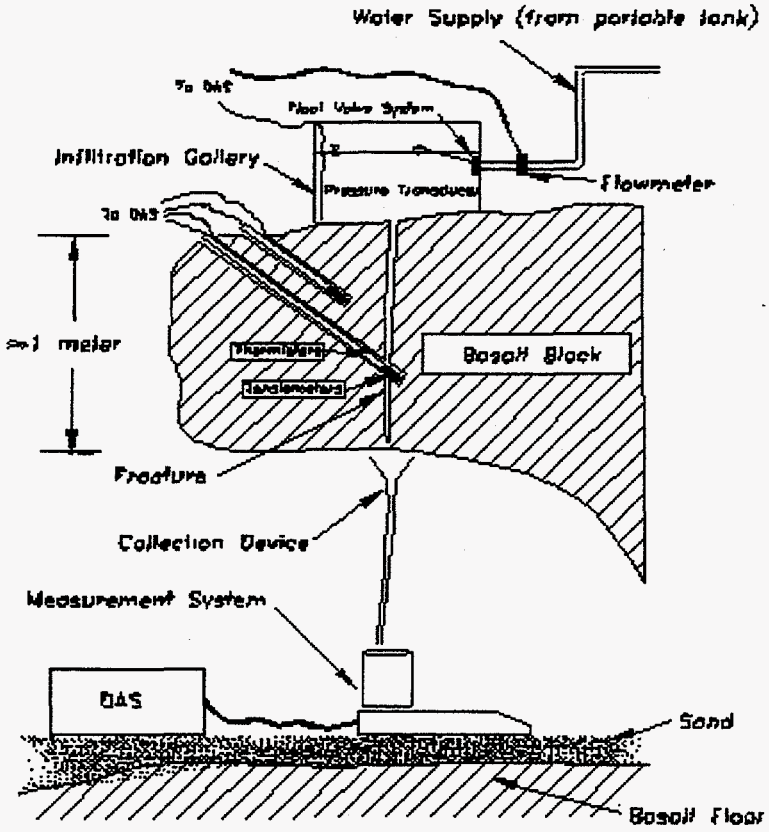

Figure 4.1. Field site characteristics and instrument layout. Note figure not to scale.

The field site was instrumented to collect data that would be amenable to a chaotic-dynamical analysis, which typically requires long time-series of data. Data collected included time stamping individual drip events for 20 distinct drip locations (to perform an analysis similar to that in Shaw, 1984); measurements of the inflow and outflow rates into the system (to compare temporal and spatial variability as well as do mass balance calculations); and moisture tension, temperature, and barometric pressure (to examine and compare with flow and drip data).

4.1 Field Test Setup and Instrumentation

Field work at the site began in June 1997 and continued until October 1997. Seven ponded infiltration tests were conducted, each with 4 to 48 hour duration and a varying amount of dry-out time (hours to weeks) between tests. Individual drips were monitored as they landed, using an array of specially designed piezo-electric sensors that sent a signal to the data acquisition system in response to the pressure increase accompanying a landing drip.

4.2 Field Observations and Preliminary Data Analysis

Preliminary reductions indicate that between 0 and 20,000 drips were collected for each location during each test. During the later tests (4-7) over 5,000 drip events were recorded at approximately 50% of the drip locations. The parameters of moisture tension, temperature, barometric pressure, and flow rates/water levels were collected at 1 minute intervals for the duration of the tests.

As the data analysis has yet to be conducted, a detailed discussion of the results cannot be presented at this time, however the following were observed during the testing:

- Flow rates were observed to vary between and during tests, ranging from near negligible inflow rates to as high as 0.8 l/min;
- The ambient moisture conditions in the basalt may exhibit some control on the flow through the fracture;
- Temporal and spatial variability was observed in the location of the first appearance of drips.

5.0 BOX CANYON PULSED PONDED INFILTRATION EXPERIMENT (LBNL)

The Box Canyon, Idaho experiment consists of a series of pulses of ponded infiltration, in which a fixed volume of water containing a known concentration of tracer (potassium bromide) is added to the pond all at once, allowed to infiltrate for two days, then pumped out of the pond, allowing air to enter the subsurface. This sequence of water and air boundary conditions is believed to be conducive to the development of chaotic flow and chemical transport behavior in the fractured basalt. In addition to monitoring water infiltration and evaporation rates from the pond, two types of measurements were conducted in the subsurface below the infiltration pond in order to study the flow and transport behavior in fractured basalt. First, time series of measurements at point locations were collected, to study the local dynamics of flow and transport and examine it for chaotic behavior. Second, snapshots of the spatial distribution of moisture and tracer movement were collected with geophysical techniques, to study the geometrical pattern of flow and transport and examine it for evidence of fractal geometry.

5.1 Infiltration Tests and Pond Data Collected

Three pulse infiltration tests of approximately 48 hours each were conducted in September-October 1997. Table 5.1 shows specifics for each test.

Table 5.1. Pulsed ponded infiltration tests conducted at Box Canyon in 1997.

Beginning of ponding		Test number	Volume added (m^3)	Duration of ponding (days)	Volume infiltrated and evaporated (m^3)
9/11/97	12:15	1	11.23	2.02	5.55
9/18/97	14:56	2	11.03	2.08	5.37
10/2/97	15:40	3	11.00	2.01	4.63

Potassium bromide slurry was added to the tanks before each test resulting in a concentration of approximately 3 mg/L. Water samples were taken from the tanks and the pond once infiltration began to check for uniformity of concentration. Analysis of these water samples is ongoing.

Water levels in the pond were measured and cumulative infiltration rates accounting for evaporation were calculated for each test. Evaporation was monitored using a pool within the berm walls. As can be seen from the final column of Table 5.1, the cumulative flow rate into the pond decreased from pulse to pulse.

5.2 Point Measurements

Time domain reflectometry (TDR) measurements were taken during the three infiltration tests and during dormant periods. During infiltration, measurements were taken every 15 minutes, and during dormant periods, every 1 or 2 hours, depending on the length of time between the tests.

Electrical resistivity (ER) measurements using miniature ER probes were taken at 15 minute intervals during and between tests. Forty-five existing probes installed at multiple depths in 5 wells were used as well as newly installed single probes placed in the bottom of 3 wells. Thirteen probes were placed within the pond, and 1 probe was placed in the water tank.

Tensiometry measurements of water pressure were done using 26 tensiometers installed within and outside the pond.

Water sampling was conducted using suction lysimeters installed in boreholes. Sampling was carried out a total of 17 times. The purpose of the sampling was to detect the movement of the bromide tracer, and construct breakthrough curves as the water infiltrated downward through the fractured basalt. Analysis of the water samples is ongoing.

5.3 Geophysical Measurements

Neutron well logging provides a one-dimensional picture of moisture distribution. It was carried out in 7 wells 10-12 times before, during, and after each ponding period. Preliminary results indicate increases in water content during infiltration in wells located within and close to the pond.

Cross-borehole ground penetrating radar (GPR) provides a two-dimensional tomogram of moisture distribution by using variations in the velocity of electromagnetic waves with dielectric constant. GPR surveys were conducted between six different well pairs. Preliminary analysis confirms that ambient conditions are wetter this year than last year, but radar tomograms still identify the central fracture zone and the rubble zone as low velocity zones.

Electrical resistivity tomography (ERT) provides a three-dimensional picture of the subsurface electrical conductivity distribution, which may be related to moisture distribution. ERT measurements were provided by Steam Tech, Inc. These measurements involved the development of special ER probes installed in three deep (20 m) boreholes outside the pond, three shallow (2 m) boreholes within the pond, and 15 surface ER probes. The data analysis is ongoing.

6.0 Non-Linear Dynamical Processes in Unsaturated Fracture Flow (UNR)

Systems exhibiting chaotic behavior are characterized by the ability to make short-term predictions. Long-term predictions are impossible because of an exponential loss rate of information on the system state. We identify and develop the conditions under which chaotic behavior in unsaturated flow can be expected so that realistic limits can be placed on predictions about the future state of the system. We cast the problem in terms of thin film flow in fractures with aperiodic saturation events using Navier-Stokes governing equations. Initial conditions consist of constant inflow rates at the top of the fracture. If the rates are small enough and surface tension dominates, the thin film will reach a steady flow rate. Above a certain threshold flow rate, as gravity begins to dominate, periodic solitons develop. Above still another threshold, aperiodic solitons take over, and the flow characteristics are chaotic.

7.0 Estimating Total Mass of Contaminant Plumes from Sparse Well Data (LBNL)

A major problem we encounter in trying to develop models (chaotic or otherwise) for flow and transport in fractured basalts is that it is extremely difficult to develop a picture of the overall spatial structure of these processes from isolated point measurements, due to the extreme heterogeneity of the system.

We consider the estimation of the total mass of a contaminant plume as a model problem to investigate means of using sparse data effectively. Generally, the estimation of the volume or mass and shape of the plume is based on sampling and analyzing water and soil. We have generated several complex hypothetical contaminant plumes. We then test the ability of different prediction methods and different sample spacing to estimate the mass of the contaminant plume. Comparisons among the methods should tell us something about the performance of different estimation methods for different types of complex distributions. They should also indicate what resolution of sampling is required to make an acceptable mass estimation.

7.1 Methods

We approach the problem of sample minimization by using several simulated heterogeneous distributions obtained from fractal generating algorithms, and a real distribution obtained from a fracture infiltration experiment. We initially select 15 well locations, based on a quasi-random scheme, along a two-dimensional cross-section. The extension of this approach to three dimensions would involve taking several two-dimensional cross-sections. The wells are sampled at equally spaced vertical intervals. Sequential predictions of the total mass of contaminant are computed as each successive well is sampled. Figure 7.1 shows the fractal plume and the wells used to sample the field. The numbers indicate the sequence in which the wells are sampled.

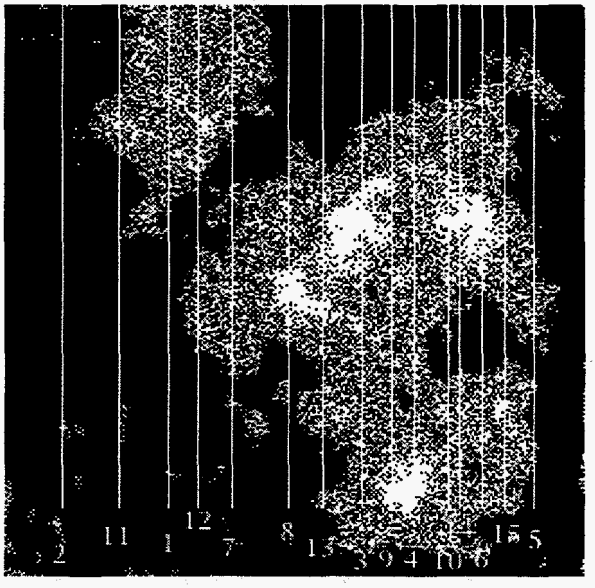

Figure 7.1. Synthetic contaminant plume with fractal geometry and locations of sampling wells.

We use several estimation techniques such as simple averaging, spatial integration, fractal and neural network models, to predict the total mass of the plume from the sample data. Parameters of the concentration distribution for the plume determined from the sparse well data were compared to those for the computer-generated plume. The convergence of the estimated plume mass to the

actual known mass, as well as the number of wells required for convergence, were used as criteria to compare the different methods.

7.2 Preliminary Results

Analyzing the concentration distribution, we found little or no spatial correlation between samples collected from adjacent wells, indicating that the wells are far enough apart to provide independent information. In general, for the examples we studied simple averaging, spatial integration, and neural network predictions performed comparably well and estimates of total mass did not significantly improve after five wells had been sampled. In contrast, the fractal-based methods proved less successful, in part because they depend strongly on the value of the fractal dimension of the plume, which is very difficult to determine from sparse well data. A comparison of some of the estimation methods is plotted in Figure 7.2 for a synthetic fractal plume with a fractal dimension prescribed to be 1.5. This plot shows how the estimation changes as each additional well is sampled. The bar indicates a perfect estimation. Interestingly, the least successful method is a fractal-based method that assumes a fractal dimension of 1.5, supposedly the actual fractal dimension of the plume. The much better performance of a fractal method that uses a fractal dimension of 1.3 suggests that perhaps the algorithm used to create the plume does not actually produce the desired fractal dimension. This topic is currently under investigation.

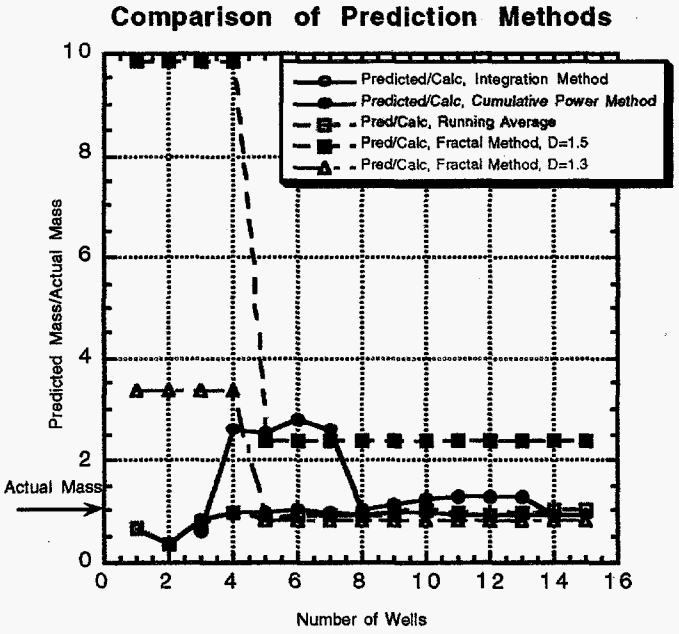

Figure 7.2. Summary of predictions for a fractal plume with a fractal dimension prescribed to be 1.5. The curves labeled cumulative power method, fractal 1.5, and fractal 1.3 all use various forms of fractal-based approaches.

8.0 TOPICS OF ON-GOING RESEARCH

8.1 Theoretical

- Study the physics of water flow and chemical transport in fractured rocks using dynamical models of chaos theory, fuzzy logic, and a combined fuzzy-chaotic approach (a tool for managing and optimizing remediation activities under conditions for which chaotic processes are important).

- Use fractal and neural network approaches to determine three-dimensional spatial distributions of properties or processes in soils and fractured rocks from point-type measurements in boreholes.

- Apply the theory of linguistic variables to lithological analysis of data from boreholes.

- Re-examine water flow and tracer transport in fractured basalt from the Large-Scale Infiltration Test in light of chaotic dynamic models.

- Compare laboratory and field methods for the determination of quasi-saturated hydraulic conductivity of soils, and use a deterministic-chaotic model to describe a variable hydraulic conductivity within the zone of fluctuation of water table.

- Examine the relationship between the spatial structure of geologic heterogeneity (using methods of fractal geometry) and chaotic dynamics, as related to infiltration through a fractured basalt vadose zone.

- Construct and investigate fractal structures created with iterated function systems (IFS), which can simulate realistic characteristics of natural fracture patterns in basalt.

8.2 Experimental

- Evaluate the performance of tensiometers in fractured rocks, using laboratory cores and modeling, taking into account the interaction between the matrix and fractures.

- Use ground penetrating radar to investigate flow in soils and fractured rocks.

- Use 2-D and 3-D ERT to evaluate zones of preferential flow in fractured rocks.

- Conduct a series of pulsed infiltration tests at Box Canyon and Hell's Half Acre field sites in Idaho.

9.0 REFERENCES

Carr, J.R., 1989. Fractal characterization of and joint surface roughness in welded tuff at Yucca Mountain, Nevada, in Proceedings of the Thirtieth U.S. Symposium Rock Mechanics, Morgantown, West Virginia, A.W. Khair, ed. (Balema, Rotterdam), pp. 193-200.

Cheng, Z., S. Redner, P. Meakin, and F. Family, 1989. Avalanche dynamics in a deposition model with "sliding," Physical Review A, vol. 40, no. 10, pp. 5922-5935.

Cox, B.L. and J.S.Y. Wang, 1993. Fractal analysis of anisotropic fracture surfaces, Fractals, vol. 1, no. 13, pp. 547-559.

Geller, J. T., G. Su and K. Pruess, 1996. Preliminary Studies of Water Seepage through Rough-Walled Fractures, LBNL Report 38810, July.

Hatano, R. and H.W.G. Booltink, 1992. Using fractal dimensions of stained flow patterns in a clay soil to predict bypass flow, Journal of Hydrology, vol. 135, pp. 121-131.

Kapitaniak, T., 1988. Chaos in Systems with Noise, World Scientific, Teanick, N.J.

La Pointe, P.R., 1988. A method to characterize fracture density and connectivity through fractal geometry, International Journal Rock Mech. Min. Sci. and Geotech. Abstract, vol. 25, no. 6, pp. 421-429.

Lorenz, E.N., 1982. Atmospheric predictability experiments with a large numerical model, Tellus, vol. 34, pp. 505-513.

Mandelbrot, B.B., 1977. The Fractal Geometry of Nature, W.H. Freeman and Company, New York.

Moon, F.C., 1987. Chaotic Vibrations, an Introduction for Applied Scientists and Engineers, John Wiley, New York.

Nicolis, G. and I. Prigogine, 1989. Exploring Complexity: An Introduction, W.H. Freeman and Company, New York, NY.

Nolte, D.D., L.J. Pyrak-Nolte, and N.W.G. Cook, 1989. The fractal geometry of flow paths in natural fractures in rock and the approach to percolation, Pure and Applied Geophysics, vol. 131, nos. 1/2, pp. 111-138.

Pasternak, G.B., 1996. Assessing claims for chaos in hydrologic records, Hydrology Days, pp. 395-406.

Pelletier, J.D., 1996. Power spectral analyses of climatological and hydrological time series: Identification of the Hurst phenomenon and application to drought hazard assessment, Hydrology Days, pp. 407-422.

Rosendahl, J., M. Vekic, and J. Kelley, 1993. Persistent self-organization of sandpiles, Physical Review E, vol. 47, no. 2, pp. 1401-1447.

Schuster, H.G., Deterministic Chaos: An Introduction, Weinheim, VCH, 1989.

Shaw, R., 1984. The Dripping Faucet as a Model Chaotic System, Aerial Press, Santa Cruz, CA.

Tsonic, A.A., 1992. Chaos: From Theory to Applications, Plenum Press.

Wood, T.R., and G.T.Norrell, Integrated Large-Scale Aquifer Pumping and Infiltration Tests. Groundwater Pathways OU 7-06. Summary Report, INEEL-96/0256, Lockheed Martin Idaho Technologies Company, Idaho, 1996.

High-Resolution Definition of Subsurface Heterogeneity for Understanding the Biodynamics of Natural Field Systems:

Advancing the Ability for Scaling to Field Conditions

Principal Investigator:
E.L. Majer, Tel: 510/495-6709, Fax: 510/486-5686, email: elmajer@lbl.gov
Lawrence Berkeley National Laboratory
Mail stop 90-1116

Co-Investigator: F. J. Brockman (PNNL)

1.0 Task Description

This research is an integrated physical (geophysical and hydrologic) and microbial study using innovative geophysical imaging and microbial characterization methods to identify key scales of physical heterogeneities that affect the biodynamics of natural subsurface environments. Data from controlled laboratory and *in situ* experiments at the INEEL Test Area North (TAN) site are being used to determine the dominant physical characteristics (lithologic, structural, and hydrologic) that can be imaged *in situ* and correlated with microbial properties. Emphasis is being placed on identifying fundamental scales of variation of physical parameters that control transport behavior relative to predicting subsurface microbial dynamics. The outcome will be an improved understanding of the relationship between physical and microbial heterogeneity, thus facilitating the design of bioremediation strategies in similar environments. This work is an extension of basic research on natural heterogeneity first initiated within the DOE/OHER Subsurface Science Program (SSP) and is intended to be one of the building blocks of an integrated and collaborative approach with an INEEL/PNNL effort aimed at understanding the effect of physical heterogeneity on transport properties and biodynamics in natural systems. The work is closely integrated with other EMSP projects at INEEL (Rick Colwell et al.) and PNNL (Fred Brockman and Jim Fredrickson).

2.0 Objective

The overall goal of this research is to contribute to the understanding of the interrelationships between transport properties and spatially varying physical, chemical, and microbiological heterogeneity. The research is being carried out in both the laboratory and at DOE field sites under natural conditions. This work addresses issues that will aid in the understanding of what scales one must sample in order to design effective remediation strategies. A critical question is the existence of one or more self-averaging quantities for microbial properties. Stated in another fashion: Are the microbial properties a function of the "randomness" of the media? If so, what is the size of the representative volume at which the significant properties can be characterized? A specific goal of the research is to advance the understanding of how to effectively use the information from geophysical imaging (i.e., volumetric measurements of physical properties) to predict the effect of physical heterogeneity and fluid transport properties on microbial behavior. A key hypothesis being addressed is that nutrient flux and transport properties are key factors in controlling microbial dynamics. A related hypothesis is that complexity of the subsurface environment is also correlated to the behavior of microorganisms.

Geophysics is ideally suited for extrapolating measurements made in a borehole to the large-scale volume away from the hole. High resolution seismic measurements are being used to resolve structure at the sub-meter scale. With this information on location of fractures, layer continuity, layer thickness and other structural and lithologic features, improved predictive models on flow and transport can be developed and applied. This is then correlated to the microbial behavior and distribution. In this application, geophysical measurements are made between holes to assess the continuity and homogeneity of the intervening material at the TAN site. Seismic imaging is being done in the fractured basalts at the TAN site using advanced processing and multicomponent imaging. Specifically, several different processing approaches are being used to obtain improved information on physical properties controlling transport behavior, including,

- Conventional and advanced ray and waveform tomography,
- Using guided/channel waves,
- Using scattered energy from voids/high contrast anomalies,
- Crosswell reflection imaging.

3.0 Progress to Date of the Geophysical Imaging

During 1997 the geophysics concentrated on obtaining crosswell seismic data at the sub-meter resolution scale at several wells in the TAN area. Tomographic imaging was carried out for crosswell pairs, T-GRW to TAN-9, TAN-25 to T-GRW, TAN-25 to TAN-26, and TAN-25 to TSF-05. Inversions were produced for the T-GRW to TAN-9 and TAN-25 to T-GRW, TAN-25 to TAN-26, and TAN-25 to TSF-05 well pairs. An example is the T-GRW/TAN-9 well pair, which produces the most complete velocity tomogram (Figure 1). The ray coverage was good from 64 to 94 m, and the inversion shows little effect of any deviations of the wells. The tomographic results show three low-velocity zones: one about 2 m thick between depths of 66 and 68 m, a thicker one at a depth of 74 to 78 m, and one at a depth of 85 to 87 m which corresponds to the low-velocity zone seen in the TAN-25/T-GRW inversion. The middle low-velocity zone is the thickest and contains the lowest velocities, well below 3 km/s. The lower low-velocity zone is not well defined here.

From the seismic imaging several results are evident. The geology of the surveyed area is quite varied, with large changes in seismic velocity and attenuation with depth. From our experience in other fractured environments, this indicates extreme variability in fracture/rock properties and from past experience is an indication of fracture permeability. In all well pairs the tomography has given good resolution on structure and possible areas of "fast paths." Although there is strong evidence that the low-velocity zones imaged with the tomography are more permeable, further analysis and correlation with other data (well logs, tracer data, etc.) and refinement using corrected hole locations from deviation surveys should yield more definitive results on the actual identification of permeable pathways and structure controlling transport.

4.0 Microbial Characterization and Scale Effects

The objective of this work is to characterize small-scale variations in subsurface microbiological properties for the following purposes: providing quantitative estimates (using variogram models) of the spatial variability of these properties; and understanding the relationships between microbiological, physical, and chemical properties (using cross-correlation models). These activities will help identify to what extent geophysical and geochemical properties control the spatial variability of microbiological properties. An additional objective is to determine how the use of different sample supports affects the measurement of microbiological properties. The definition of an appropriate averaging scale is critical in providing more accurate input into

predictive models of contaminant transport and will improve the precision of the simulations. The final objective is to quantify changes in the spatial structure and magnitude of microbiological properties following the impingement of a contaminant plume. An associated objective is to determine how the contamination event affects the measurement of microbiological properties at different sample supports.

5.0 Progress to Date of the Microbial Work

5.1 TAN-33

Rock samples were obtained from one EMSP-funded borehole in FY97. Although we worked closely with personnel at INEEL , it was not possible (given their funding, schedule, and logistical considerations) to obtain the number, type, and quality of rock samples required for meeting the stated objectives. However, in FY98 we will be able to address our first two objectives based on sampling and analysis of groundwater from the borehole described above. In TAN-33, after a delay in obtaining samples from the EMSP-funded borehole, we obtained samples from a Subsurface Science Program-funded borehole to refine DNA extraction protocols in basaltic rock material. The TAN-33 borehole was located in a region containing low levels of contamination (less than 0.5 ppm trichloroethylene, TCE). Community DNA was successfully extracted from several of the rock samples, the 16S rRNA genes were amplified and cloned, and phylogenetic analysis was performed.

5.2 TAN-37

Compared to TAN-33, the TAN-37 borehole is closer to the source of contamination and contained 5-10 times more TCE. Microbial activity (determined by other investigators) in the TAN-37 borehole was much higher than in the TAN-33 borehole. DNA was extracted and successfully amplified from all rock samples to date; these samples correspond to the depths where the multi-level groundwater sampling will occur in FY98. DNA extraction is being performed on the remaining 15 rock samples from the TAN-37 borehole. Timecourse degradation (1-12 weeks) of 14C-labeled organic substrates (methane and phenol aerobically; lactate and methanol anaerobically) and 14C-trichloroethylene, in the presence and absence of additional inorganic and organic nutrients, was performed on 8 rock samples, and analysis by gas chromatography-gas proportional counting is underway.

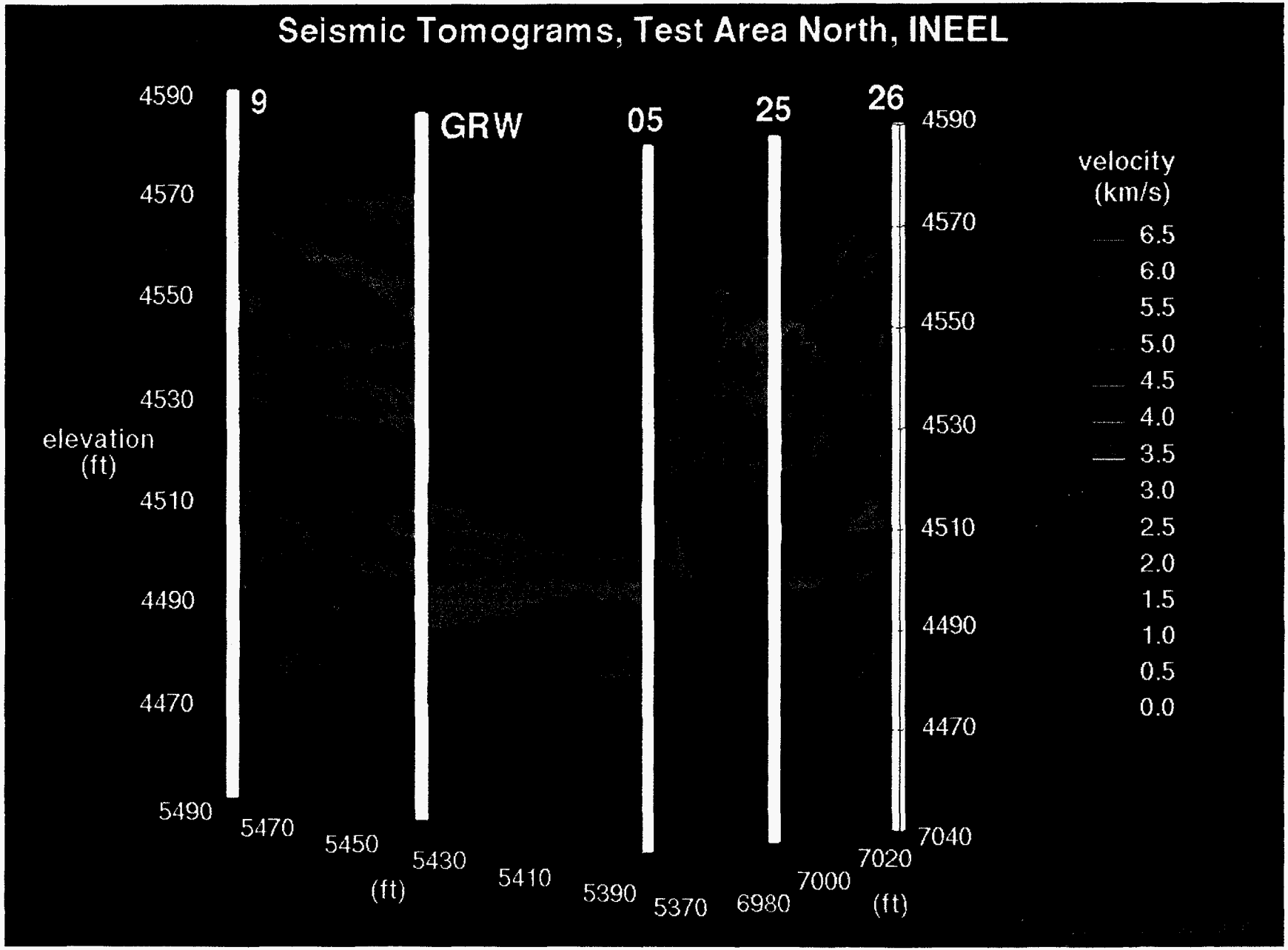

Figure 1. T-GRW/TAN-9 well pair.

Improved Analytical Characterization of Solid Waste Forms (glass, metals, soils) by Fundamental Development of the Laser Ablation Technology

Richard E. Russo, Principal Investigator

Tel: 510/486-4258, Fax: 510/486-7303, email: RERusso@lbl.gov
Lawrence Berkeley National Laboratory
Mail Stop 70 - 193A
Berkeley, CA 94720

EXECUTIVE SUMMARY

Laser ablation is a promising technology for chemical characterization within every DOE EM major problem area (high-level waste tanks, contaminant plumes, D&D activities, spent nuclear fuel, mixed wastes, landfills, nuclear waste disposal, and HEU disposition). This EMSP research endeavors to expand the fundamental basis in laser ablation technology for its application to these DOE characterization needs. Laser ablation must be understood on a fundamental level to ensure confidence in chemical characterization of environmental samples. The goal is to develop a fundamental understanding of laser ablation processes, and to determine the influence of these processes on analytical behavior (sensitivity and accuracy) in order to bring this technology to fruition. This report summarizes the research completed in the first year of this project. The initial work addressed: accuracy of chemical characterization by verifying that the ICP (inductively coupled plasma) was not adversely influenced by ablated mass; accuracy of ablation sampling versus laser pulse time; and sensitivity enhancements through the use of various gas environments. The research and development utilized an existing inductively coupled plasma-atomic emission spectroscopy (ICP-AES) system. Part of the effort also included the evaluation, purchase, and installation of an inductively coupled plasma-mass spectroscopy (ICP-MS) system. Three scientific manuscripts were completed and submitted to technical journals. One of the goals of this work is to support the efforts at all the national laboratories investigating laser ablation technology for the management of DOE radioactive, hazardous chemical, and mixed waste; collaborations with scientists at other national laboratories have been initiated.

1.0 INTRODUCTION

Laser ablation is a promising technology for chemical characterization within the EM program for numerous reasons. Laser ablation is a direct sampling and characterization technology; one ablates the sample and characterizes its chemical composition. The sample can be homogeneous, heterogeneous, radioactive, stable, inorganic, organic, biological, sludge, saltcake, soil, etc. Within the EM program, many of the samples will be hazardous. Laser ablation technology provides these capabilities. There is no sample preparation; therefore, laser ablation can eliminate thousands of dissolutions, eliminate additional solvent waste, minimize contamination of equipment, and minimize personnel exposure to samples and solvents. Chemical analysis using laser ablation requires a smaller amount of sample (< micrograms) than that required for conventional solution nebulization (milligrams). Depending on the analytical detection system, picogram to femtogram quantities may be sufficient for analysis, providing a pseudo

"nondestructive" analytical technology. Laser ablation can be used in the laboratory or in a field environment; it represents one of the only potential methods to perform in-situ real-time characterization of metals in diverse complex samples. The goal of this EMSP project is to develop the fundamental and experimental capabilities so that laser ablation technology can be applied to EMSP chemical characterization needs. The three separate sections below describe completed research and development in FY97.

2.0 EXPERIMENTAL LASER ABLATION SYSTEM

The experimental system for laser ablation and analysis is shown in Figure 1. The beam from a pulsed laser is directed into the "ablation" chamber and focused onto the sample surface. The ablated sample vapor is transported by gas flow to the central channel of an ICP torch. Spectral emission from the ICP is measured by a monochromator with a charge coupled device (CCD) detector. An inductively coupled plasma-mass spectrometer (ICP-MS) was purchased for this research. ICP-MS is utilized throughout the chemical analysis community because of its enhanced sensitivity and isotopic capabilities, two important parameters to the DOE chemical characterization mission. The initial research using this new instrument was obtained in the last month of the fiscal year; these data will be reported in the next annual report.

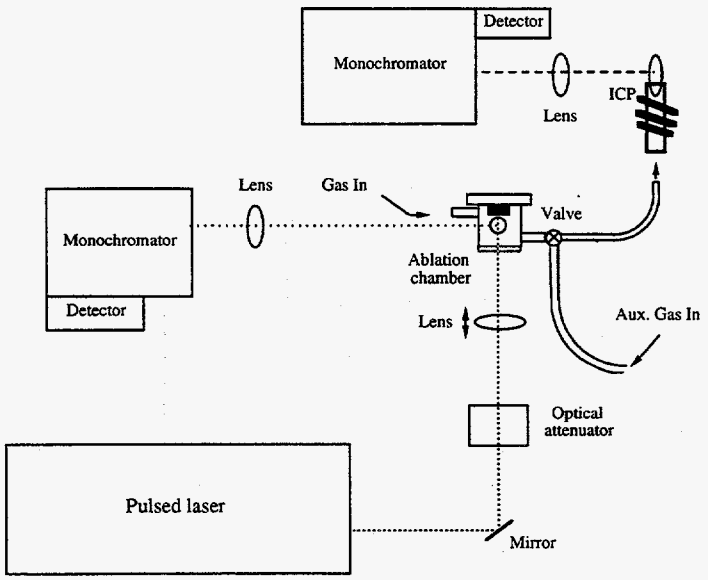

Figure 1. Diagram of LA-ICP-AES experimental system for chemical characterization.

2.1 Verification of ICP-AES Accuracy to Ablated Mass

One of the first studies we performed was to determine if the ablated sample entering the ICP affected the plasma conditions. It is critical to ensure that the ablated mass entering the ICP does not significantly influence plasma temperature and electron number density, because changes in these parameters will be manifested as changes in chemical concentration or composition; i.e., inaccurate analysis. For conventional ICP-AES analysis of solutions by means of liquid nebulization, the amount of aerosol entering the plasma is determined by the nebulizer/spray chamber parameters and does not significantly change during aspiration of standards and samples with slightly different concentrations. In contrast, the mass loading to the ICP during laser ablation sampling depends on the sample matrix and laser properties. Different amounts of ablated mass and/or dry aerosol of different particle sizes will be introduced to the ICP during laser ablation solid sampling of standards and samples.

The influence of ablated mass on the electron number density and temperature within the ICP was studied by measuring the ratio of Mg ionic to atomic emission lines and selected Fe lines, respectively. The ICP electron number density was investigated by using measurements of the Mg ionic to atomic resonant line ratios during laser ablation of an aluminum matrix. The ICP excitation temperature was measured by using selected Fe lines during laser ablation of an iron matrix. A Nd:YAG laser (3 ns pulse duration) at 266 nm with different repetition rates was used for these ablation sampling studies. Laser energy, power density, and repetition rate were varied in order to change the quantity of ablated mass into the ICP. The ICP emission intensity, which is assumed to be proportional to the amount of ablated mass, changed over approximately one order of magnitude during sampling of Al and Fe matrices. *A priori*, self absorption for the spectral lines used in the measurements was always checked.

The experimental system was described above. Elemental spectral emission was measured over the entire vertical length of the ICP. The ICP operated at gas flow rates of 14 l/min for Ar plasma gas, 1.0 l/min for auxiliary gas and 0.2 l/min for central carrier gas. The Nd:YAG laser was operated at 266 nm with 3 ns pulse duration. Laser repetition rate was 10 Hz unless otherwise specified. The laser energy used in these studies was 5 mJ and 10 mJ, and was monitored continuously during the experiments. The reproducibility of the laser energy from shot to shot was approximately 5%.

The samples consisted of either an aluminum matrix with a small amount of Mg (95% Al, 4% Cu, 1% Mg) or pure Fe samples (99.999%). These samples were chosen strictly to verify the ICP behavior; environmental samples are expected to behave similarly, but would present more complex spectra and significantly complicate these studies. The Al sample was chosen for the measurements of the ratio of magnesium ion to atom resonance lines. The pure Fe sample was used in measurement of the ICP temperature. A pure MgO (Pure Tech Inc., 99.9%) sample was used to demonstrate self-absorption effects.

2.1.1 Measurement of the Mg Ionic to Atomic Emission Ratios

It is well known that the ionic to atomic spectral intensity ratio for the same element can be used to measure the "energy characteristics" of the ICP discharge. The fundamental expressions for calculating these parameters are beyond the scope of this report and can be found in Ciocan et al. (under submission). The data in Figure 2 show this ratio over the entire vertical extent of the ICP for different laser power densities. The Mg II 279-nm/Mg I 285-nm changes by more than a factor of 3 along the ICP central axis. This change corresponds to the axial inhomogeneities of

the ICP temperature and electron number density. However, there are no significant changes of this ratio at different laser power densities at any height above the load coil. The scatter of the data in the region below the load coil are due to the weak Mg atomic emission line intensity in this region. The possibility of self absorption of these spectral lines was checked. This determination is essential, especially when working with resonant lines or even with nonresonant lines that belong to the matrix. The ratio remains constant over this range of laser power densities, proving that both resonant Mg lines are optically thin and no self absorption results. The Mg II 279-nm and Mg II 280-nm lines are almost "ideal" to check for self absorption, since they have very close upper excitation levels.

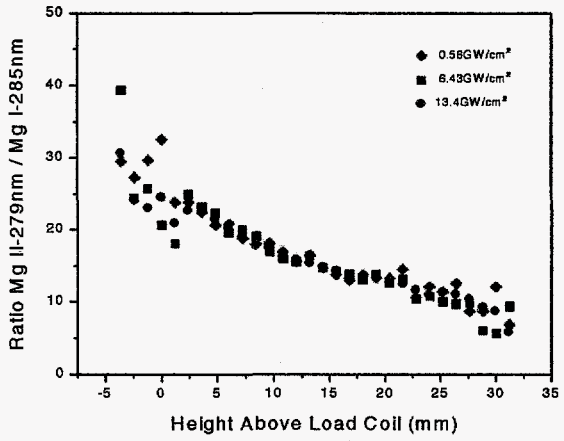

Figure 2. Ratio of Mg ionic to atomic emission in the ICP versus height above load coil for several laser power densities.

If the ICP is not perturbed by the ablated mass, plasma temperature should not change. In this case, the optical emission signal will be proportional to the amount of ablated mass entering the ICP. In Figure 3 the ratio of Mg II/Mg I is plotted versus the relative intensity of Al I 257-nm, which is proportional to the amount of ablated mass. The ratio remains constant within the error over approximately an order of magnitude change in the Al emission intensity. Al I 257-nm was selected as an indication of the total ablated mass, since it is a matrix line and the standard deviation from shot-to-shot ablation is less than for a minor component such as Mg. In addition, the concentration of Mg is given over a large range (0.2%-0.8%); inhomogeneities in the bulk can be expected to contribute to the error. The stronger Al emission line is a more reliable indication of the ablation process, as long as the line is not self absorbed. Here, the Al I 257-nm has been confirmed to be free of self-absorption. The line used for checking self absorption was Al I 265 nm, which has a very close upper state energy with Al I 257-nm.

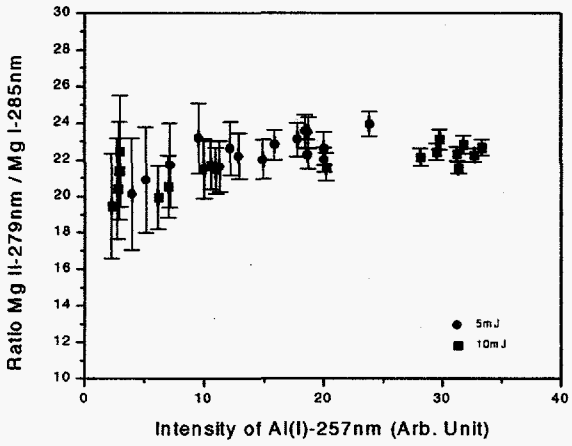

Figure 3. Ratio of Mg ionic to atomic emission versus the ICP Al emission line intensity.

In previous studies from this research group, roll-off and nonlinear dependence were observed in ICP intensity normalized to laser spot area, versus laser power density. If the roll-off and nonlinear dependence are not caused by changes in ICP conditions due to mass loading, then these ICP data represent fundamental laser ablation processes. The ratio of Mg II/Mg I versus laser power density was the same over the range of laser power densities used in this experiment. These data confirm that the roll-off and nonlinear dependence are caused by laser ablation sampling and not by changes in the ICP conditions.

2.1.2 ICP Excitation Temperature Measurements

The ICP temperature calculated during ablation using the different laser power densities is shown in Figure 4. Here we show the error bars arising only from measurement uncertainties, rather than error bars reflecting uncertainties in Einstein coefficients. ICP excitation temperature does not change within the experimental errors. However, nonlinear mass ablation rate and roll-off were observed during laser ablation sampling of the Fe sample over this power density range; the ablation rate changes by two orders of magnitude. ICP temperature remains constant over this power density region, supporting our belief that the roll-off and nonlinearity are not caused by changes in ICP conditions from different amounts of mass. These results are also supported by other nonspectral emission-based measurements in which roll-off and nonlinearity were observed.

In order to increase the amount of ablated mass entering the ICP, the laser repetition rate was varied from 5 to 50 Hz, at a constant laser power density. The ratio of Fe I 386.0-nm to Fe I 381.6-nm exhibits a constant value within experimental error. These data demonstrate that the ICP temperature does not change when the ablated mass entering the plasma is increased by a factor of 10. The ICP temperature was measured under two experimental conditions for increasing the ablated mass: 1) fixed repetition rate of 10 Hz with increased power density, and 2) fixed power density with increased repetition rate. For both cases, the temperature was not influenced by mass loading.

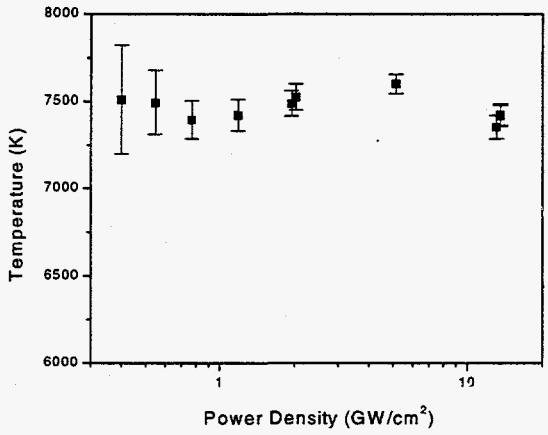

Figure 4. Excitation temperature in the ICP versus laser power density calculated using the two-line method.

2.2 Time-Resolved Studies of Mass Effect on ICP-AES

The quantity of ablated mass and its relative composition of elemental components strongly depend on the number of laser pulses at the sample surface (Borisov et al., under submission). For chemical analysis, the quantity of mass removed determines the signal intensity measured in the ICP-AES; a change in quantity can be misinterpreted as a change in chemical concentration. The mass ablation rate (quantity) *versus* time is an important parameter and is influenced by the sample surface oxide layer, extended heating and melting of the sample, and crater formation. These parameters can be studied by measuring the ICP-AES emission intensity as a function of time during repetitive ablation sampling. Preferential vaporization (fractionation of components based on volatility) during laser ablation sampling can be a problem for chemical analysis. The thermal component of laser ablation sampling influences the relative composition of the vapor, enhancing low melting-point elements in the vapor phase; the vapor is not stoichiometric and the analysis is inaccurate. Experimental conditions under which the composition of the ablated vapor is representative of the bulk sample need to be elucidated for accurate chemical analysis. Quantity and relative composition versus continuous laser sampling were investigated in this part of the work. The mass ablation rate and ablated mass composition were studied by monitoring the time dependence of emission intensity in the ICP during repetitive laser ablation at a single location on the sample. The ratio of emission lines gives an indication of the relative composition of constituents.

For this part of the work, a brass sample was ablated using several lasers with various conditions. The lasers used are the KrF excimer with a 30-ns pulse width, Nd:YAG with a 3-ns pulse width, and Nd:YAG with a 35-ps pulse width. Laser ablation was accompanied by nebulization of water. Aqueous aerosol and ablated vapor were combined at an exit port of the ablation chamber using a T-connector and directed into the ICP for analysis. By nebulization of brass standard solution, the Cu-to-Zn ratio was used as a reference for laser ablation experiments. Cu 224.7-nm and Zn 206.4-nm ionic emission lines were used in all these experiments.

2.2.1 Time-Resolved Studies of Mass Ablation-Rate Dependence on Laser Fluence

The data in Figure 5 show Cu II 224.7-nm line emission intensity time profiles. Generally, higher laser fluence provides higher overall ICP emission intensity, which corresponds to a larger mass ablation rate. Cu emission intensity stabilized after about 2 min when the brass sample was ablated with 308-nm excimer (30-ns) laser pulses (Fig. 5a). However, at the lowest fluence of 0.84 J/cm^2, Cu emission intensity increases slowly and stabilizes at values larger than those for higher fluences of 2.40 and 3.24 J/cm^2. This behavior may be explained by an increased degree of elemental fractionation at the low fluence. At a fluence of 0.84 J/cm^2, sampling (ablation) takes place from a large surface area. Melting and preferential vaporization of Zn can result in significant enrichment of Cu in the crater. Cu enrichment was confirmed by energy-dispersive X-ray spectroscopic (EDX) measurements performed in the laser ablated crater. After about 4 minutes of continuous ablation, sampling takes place from a Cu-rich surface. Zn emission intensity shows the opposite behavior (not shown here), confirming this phenomena.

By using the 3-ns pulses from the Nd:YAG laser (Fig. 5b), Cu emission intensity stabilizes after 20-30 s of ablation at low fluences, indicating a constant or steady rate of mass ablation. However, at higher fluences of 4.40 and 15.0 J/cm^2, emission intensity increases continuously as the crater is formed. Zn intensity (not shown here) follows that of Cu, indicating an increase in the mass ablation rate with time. This behavior can be attributed to a "small spot effect". At these high fluences, the crater becomes narrow and deep (approximately 50 μm in diameter and 1 mm in depth) after 3 min of ablation. It may be that molten droplets are ejected into the Ar flow due to the high pressures at the bottom of the crater. Alternatively, for deep craters the laser-induced plasma can form directly inside the crater and can be responsible for increased mass ablation rate, by sputtering or radiative heating from the plasma.

Ablation with 35-ps laser pulses resembles the 3-ns case, with indication of a "small spot effect" at higher fluences (Fig. 5c). At low fluences, time profiles of Cu emission intensity have a peaked shape, which is not characteristic of ablation with 3-ns laser pulses. The peak-shaped mass ablation rate behavior may result from the influence of the crater aspect ratio on the vapor phase expulsion of mass. In addition, as the crater develops, the fluence effectively changes and, hence, changes of the mass ablation rate can occur.

2.2.2 Zn-to-Cu Mole Ratio Time Profiles

Figure 6 compares time-resolved Zn/Cu mole ratios measured during ablation with the different lasers at various fluences. Generally, after approximately 30-40 s of ablation, the ratios stabilize, indicating constant composition of the vapor phase. However, at low fluence of 0.84 J/cm^2 for 30-ns excimer laser ablation, the plume is initially enriched with Zn and the ratio only slowly decreases to its constant value as the sample surface becomes Cu-enriched. A characteristic feature of ablation with the 30-ns pulse excimer laser is a large spread for Zn/Cu ratios, especially at low fluences, indicating a strong thermal interaction (Fig. 6a). The y-axis in Fig. 6a is a *log* scale compared to the linear axis for Figs. 6b and c. The ratios are much more stable and less dependent on fluence when ablation was performed with the 3-ns and 35-ps Nd:YAG lasers. Although the mass ablation rate at high fluences increases with time (Figs.5b and c), the Zn/Cu ratio is relatively stable, indicating small time variations of vapor phase composition. However, in all the cases, the ratio of elements in the vapor phase is highly influenced by the laser fluence.

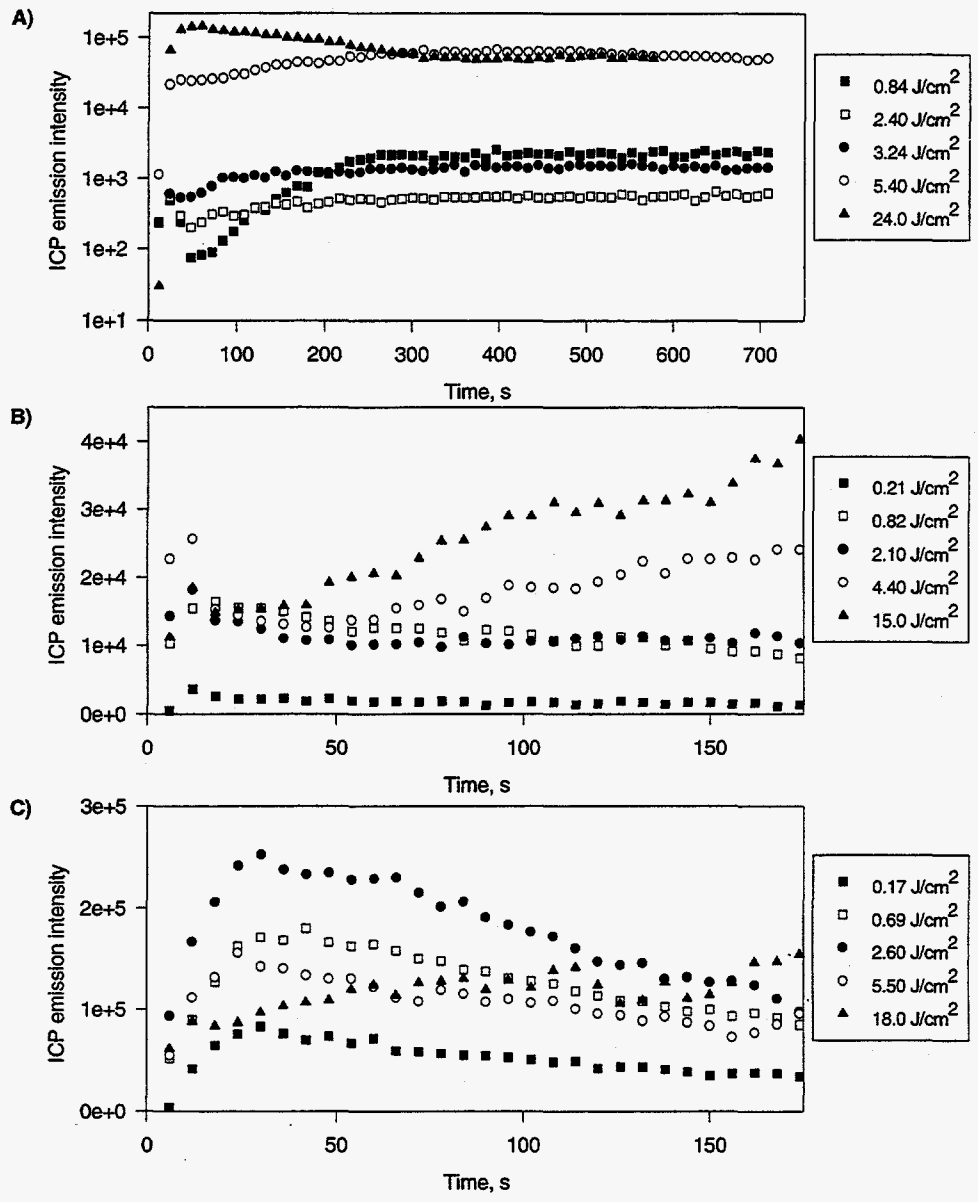

Figure 5. Cu (II) 224.7-nm ICP-AES emission intensity time profiles, measured during continuous ablation with 30-ns KrF excimer (A), 3-ns Nd:YAG (B), and 35-ps Nd:YAG (C) lasers at various fluences as indicated in the legends. Each point on the graph is a six-second integrated ICP intensity.

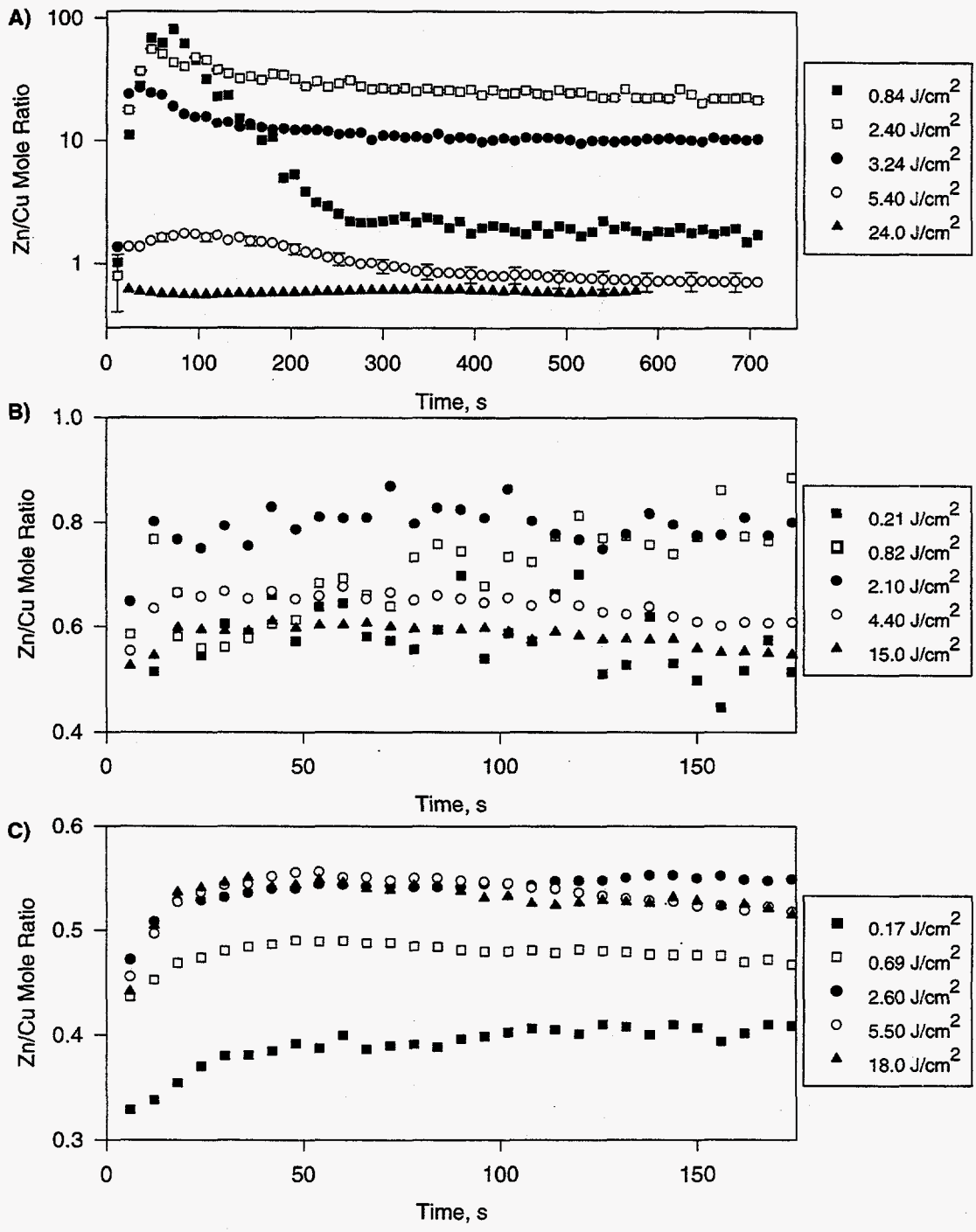

Figure 6. Zn-to-Cu mole ratios time profiles, measured during continuous ablation with 30-ns KrF excimer (A), 3-ns Nd:YAG (B), and 35-ps Nd:YAG (C) lasers at various fluences as indicated in the legends.

2.3 *Effects of Gas Environment on Pico-Second Laser Ablation Sampling for ICP-AES*

During laser ablation, the sample is contained in a chamber with a flowing gas stream at atmospheric pressure. The laser beam passes through the gas atmosphere before reaching the sample surface. The gas atmosphere, therefore, may have a strong influence on the laser ablation process and affect the efficiency of laser sampling. In this part of the research, the effects of gas medium on pico-second laser ablation sampling were studied for enhancing ICP-AES sensitivity. Five noble gases were used in the laser ablation sampling chamber. These five gases represent a relatively large range of ionization potential (IP), atomic mass, and thermal conductivity. Since the temperature and excitation characteristics of a mixed gas ICP change with the gas type, analyte spectral line emission intensity and ICP vertical emission profile shape may also change. To ensure a valid comparison of the gas effects on laser ablation, ICP emission spectra and ICP vertical spatial profiles for laser sampling in different gases were measured and the effect relative to laser sampling in Ar was reported (Chan et al., under submission). Ar is used as the reference because it is the most commonly used carrier gas for the ICP and has a medium ionization potential among the five gases.

The experimental system consists of a picosecond Nd:YAG (1064 nm) for laser sampling, the inductively coupled plasma (ICP), and the imaging spectrometer with a CCD detector for ICP vertical profile emission intensity measurement. Laser power densities of 7 to 70 GW/cm^2 were used. A stream of carrier gas passes through the chamber to deliver the laser-sampled material to the central channel of the ICP torch *via* a Teflon tube (6 mm in diameter and 1 m in length) (cf. Fig. 1). There are two carrier gas streams. One gas stream passes through the ablation chamber to sweep the laser-sampled material out of the chamber into the ICP. The second gas stream combines with the first stream at the exit of the chamber *via* a T-joint. The flow rates of both gases were 0.5 L/min, i.e., the combined gas flow rate was 1 L/min. The first stream of carrier gas that passes through the laser sampling chamber is called "chamber gas"; the second stream is called "makeup gas."

Five noble gases (He, Ne, Ar, Kr, and Xe) were used. The noble gases were always paired with Ar as a makeup gas - chamber gas pair. Two identical sets of measurements for each gas pair were performed. The ICP-AES emission intensities were ratioed to determine the effect of the noble gas on laser sampling relative to Ar. Since the gas composition in the ICP was kept constant, the effects of gas medium on ICP excitation characteristics are canceled by ratioing the two intensities. All five possible pairs of gases were used, namely, He-Ar, Ne-Ar, Ar-Ar, Kr-Ar and Xe-Ar.

Brass samples (35 % Zn and 65 % Cu) were used for the entire study. All samples were polished with 300-grit sand papers and cleaned with distilled-deionized water before sampling. For each measurement, a fresh spot on the sample surface was used. Each spot was pre-ablated for one minute (i.e. 600 laser pulses) to obtain a steady mass ablation rate before measurement of the ICP emission intensity.

Using He as the chamber gas, Cu I and Cu II are enhanced by 6 times, but Zn II is enhanced by 20 times. The difference in intensity ratios for Cu *versus* Zn is smaller using Ne, Ar, Kr, and Xe: 10-20%. There is twice the enhancement in sensitivity in Ne and a 20% reduction in sensitivity for Xe. These experiments demonstrate that the quantity of ablated mass can be significantly

enhanced by using a small percentage of helium in the ablation chamber. An increased quantity of mass provides stronger analytical AES intensity, which in turn provides enhanced sensitivity.

3.0 CONCLUSION

In this initial year of research, we studied and demonstrated three very important components of laser ablation sampling for chemical characterization. In one study, we demonstrated that the ICP-AES technology is accurately responding to the chemical composition. The ratio of Mg ionic to atomic emission lines and Fe atomic emission line pairs were used to confirm that ICP conditions do not change with different amounts of ablated mass. By changing the laser beam properties and thereby the ablation conditions, the amount of ablated mass was changed over approximately an order of magnitude. Under these experimental conditions, the ICP was not perturbed by different amounts of mass. The plasma conditions remained constant proving that the ICP can be used for accurate chemical analysis over a large range of laser operating conditions. Such a study has never been performed and clearly confirms the robustness of the ICP for representing laser ablated mass. With this information, analysts can rely on the concentration and composition changes measured in the ICP.

In a second study, we demonstrated how the quantity and composition of ablated mass changes during time as the laser repetitively removes mass from the sample. The quantity of ablated mass and its composition strongly depend on the number of laser pulses and laser fluence at the sample surface. It is important for the analyst to be aware of these effects as the reported chemical composition can be greatly influenced by time and laser power density.

Finally, we demonstrated how the efficiency of laser sampling can be improved by simply using a different gas in the ablation chamber. In this case helium provided the greatest enhancement. The noble gases (He, Ne, Ar, Kr, Xe) influence the ICP excitation characteristics and the sampling efficiency significantly. The significant enhancement in ICP sensitivity in He is due to a convolution of the effect of higher He mixed gas ICP temperature and laser sampling efficiency. The improvement in sampling efficiency is beneficial to chemical analysis especially for trace analysis which requires high sensitivity.

4.0 MANUSCRIPTS RESULTING FROM THIS WORK AND SUBMITTED TO TECHNICAL JOURNALS

A. C. Ciocan, X. L. Mao, Oleg V. Borisov and R. E. Russo. Optical Emission Spectroscopy Studies of the Influence of Laser Ablated Mass on Dry Inductively Coupled Plasma Conditions, submitted to Spectrochimica Acta, April 1997.

V. Borisov, X. L. Mao, A. C. Ciocan, and R. E. Russo. Time-Resolved Parametric Studies of Laser Ablation Using Inductively Coupled Plasma Atomic Emission Spectroscopy, submitted to Applied Surface Science, July 1997.

W.T. Chan, Amy P.K. Leung, X.L. Mao and R.E. Russo. Effects of gas environment on pico-second laser ablation sampling for ICP-AES, submitted to Applied Surface Science, July 1997.

Environmentally-Induced Malignancies: An *In Vivo* Model to Evaluate the Health Impact of Chemicals in Mixed Waste

Principal Investigator: Maria Pallavicini,
Tel: 510/486-6124, Fax: 510/486-5735, email: mgpallavicini@lbl.gov

Lawrence Berkeley National Laboratory
Mail Stop 934-47A

1.0 OBJECTIVE

Occupational or environmental exposure to organic ligands, solvents, fuel hydrocarbons, and polychlorinated biphenyls is linked to increased risk of developing leukemia, a blood cancer. The long term health effects of exposure to complex mixtures of chemicals and radionuclides are of particular concern because their biologic effects may synergize to increase risk of malignancy. Increased understanding of steps in the progression pathway of a normal cell to a cancer cell is important for biomonitoring, risk assessment and intervention in exposed individuals.

2.0 APPROACH

Leukemias are characterized by multiple genetic aberrations. Accumulation of multiple genomic changes may reflect genomic instability in the affected cells. Thus agents that induce DNA damage or genomic instability may increase accumulation of genomic alterations, thereby predisposing cells to transformation. However, not all DNA damaging agents predispose to transformation. Other factors such as genetic susceptibility, cell and tissue response to genotoxicity and cytotoxicity, and DNA repair will impact malignant progression. We proposed a progression model (Figure 1) of environmentally-induced leukemia that can be evaluated using mouse models.

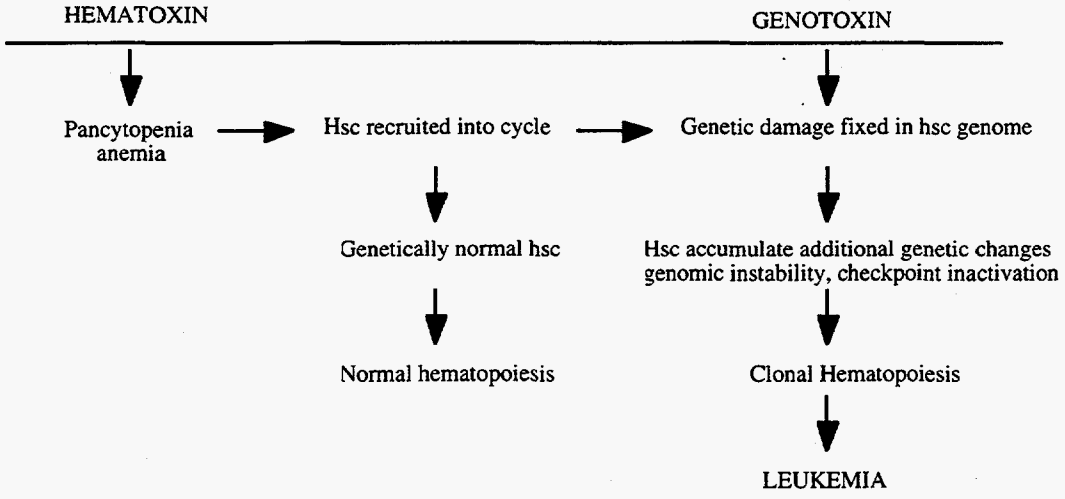

Figure 1. Model of Environmentally-Induced Leukemia

Critical components of this model include induction of genomic changes in stem cells (the population responsible for maintaining lifetime blood cell production), accumulation of additional genetic changes in stem cell progeny, and cell cycle check point inactivation. Importantly, the model postulates that mixtures of chemicals that kill blood cells and are genotoxic will synergize to increase

the frequency of cells with genomic changes, and thus increase the risk of transformation. Although stem cells are normally quiescent, they are recruited into cycle following hemotoxic insult, thereby facilitating generation of progeny with altered genomes. Chemicals that increase the rate of genomic instability in hemopoietic stem cells (hsc) are likely to increase the frequency of hsc and progeny with altered genomes.

3.0 Results to Date

This model assumes that the genetic alterations in leukemic blast cells will be present in stem cells, which are precursors to blast cells in normal hematopoiesis. Indeed, we demonstrated that stem cells in marrow aspirates from patients with leukemia carry similar genomic aberrations as the leukemic cells. We next determined whether exposure to radiation induces genomic changes in stem cells in mice. In these studies, we isolated stem cell populations from bone marrow using cell sorting from mice that were exposed to radiation one year prior to harvest. Genomic damage was measured using fluorescence *in situ* hybridization to detect translocations, stable structural chromosomal aberrations in the isolated stem cell populations and lymphocytes. We demonstrated that few stem cells from mice that do not develop radiation-induced leukemia carry translocations. Studies are underway to measure translocations in stem cells of mice that are genetically susceptible to radiation and benzene-induced leukemia.

The model postulates that combinations of agents that induce hematoxicity with those that are genotoxic will recruit stem cells to proliferate and thus induce genetic damage to be propagated in stem cell progeny. To test this hypothesis, we treated mice with 5-fluorouracil (5-FU), a cancer chemotherapeutic reported to recruit cells into cycle. 5-FU treated and untreated controls were then irradiated and translocations measured 3 months thereafter. We postulated that mice that received radiation and were treated with 5-FU would carry more translocations than those without stem cell recruitment. Although the frequency of lymphocytes with chromosome 11 translocations was increased compared to chromosome 2, the lymphocyte translocation frequency was similar with both treatments. Subsequent measurements of the fraction of proliferating stem cells in 5-FU treatment mice revealed that stem cells were not recruited into cycle using our treatment regime. A different drug-radiation schedule to recruit stem cells was developed and is now being evaluated in our laboratory.

We postulated that benzene and its metabolites will induce translocations in hematopoietic cells in a dose-dependent manner. We measured translocation frequency using fluorescence *in situ* hybridization to paint individual chromosomes and fluorescence microscopy to quantify the number of cells in which the painted chromosomes translocated to an unpainted chromosome.

Examples of a chromosome painting in an unexposed cell and a cell exposed to benzene are shown in Figure 2a and b, respectively.

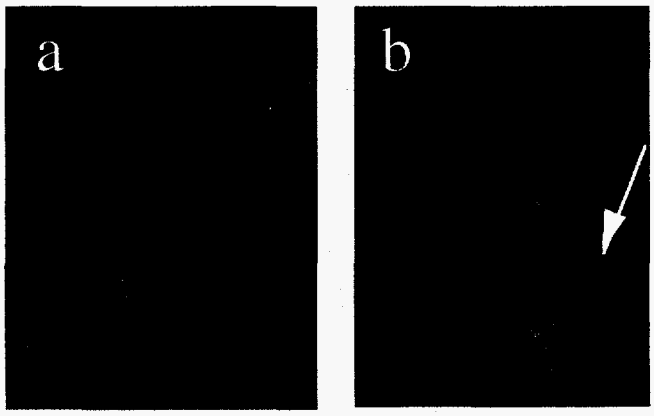

a. Normal cell with chromosome 2 (red) and 11 (green).

b. Benzene-exposed cell showing a chromosome 2 translocation.

Figure 2. Translocations Detection using Chromosome Painting.

Exposure to an active benzene metabolite induces translocations in hemopoietic cells (Figure 3). Myeloid cells show more translocations than lymphoid cells. The translocation frequency appears to be maximum at a dose of 5μM. Higher doses result in cell death.

Figure 3. 4-Hydroquinone Induces Translocations in Lymphoid and Myeloid Cells

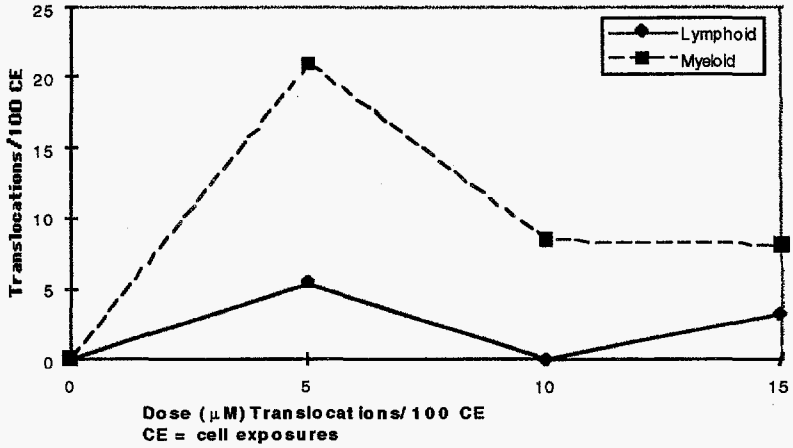

Interestingly, benzene exposure is associated with myeloid, rather than lymphoid leukemias, thus it is intriguing to speculate that cells in the myeloid lineage may accumulate more DNA damage than other cell types.

Assays for cell cycle checkpoint inactivation in hemopoietic stem cells are under development. Initial plans to use an enzyme inhibitor to assess checkpoint inactivation and genomic instability were not fruitful with hemopoietic cells. Thus, we turned to selective pressure using gamma interferon and TGF-B to isolate cells with a survival advantage and unstable genomes. These agents have been implicated recently in leukemia and myelodysplasia, a pre-leukemic condition in humans. These assays appear promising.

4.0 FUTURE WORK

Studies to be carried out during the next year will focus on evaluation of genomic instability and checkpoint inactivation induced by benzene metabolites with or without radiation using the aforementioned assays in exposed animals. Animals treated with benzene/radiation earlier in the project should be developing leukemias within the forthcoming year and thus provide suitable systems to investigate regions of the genome that are altered in environmentally-induced leukemias.

5. 0 SIGNIFICANCE

These studies will establish by proof-of-principle whether agents associated with leukemias induce genomic changes in hemopoietic stem cells. Furthermore, we will determine whether exposure to two agents (benzene and trichloroethylene) common in mixed waste at DOE sites can synergize to increase the frequency of genetically damaged cells. These data will be useful to establish mechanisms that may lead to increased risk of leukemia in exposed individuals.